Memoirs of the Faculty of Engineering, Nagoya University
Vol. 28, No. 1. (1976)

IN-SITU DYNAMIC OBSERVATIONS OF DISLOCATION BEHAVIOUR IN METALS AND ALLOYS BY HIGH VOLTAGE ELECTRON MICROSCOPY

TORU IMURA and HIROYASU SAKA

Department of Metallurgy

(Received May 31, 1976)

CONTENTS

Abstract

In order to study the dynamical properties of dislocations, a new direct method is developed which is based on the *in-situ* deformation experiment in a HVEM. Various types of device for *in-situ* deformation of foil specimens under observation in a HVEM are developed. These devices allow the continuous recording of the dynamical behaviour

of individual dislocations in the stressed crystals in the temperature range from 77K to 1123K, with the stress-strain curve being recorded simultaneously.

The motion of edge and screw dislocations is observed in thick foil specimens of Fe, Fe-3%Si, Mo and Ni being stretched (or extended and compressed alternately) at various temperatures in a HVEM operated at 400 kV-1000 kV. By establishing a direct correlation between the dynamical behaviour of individual dislocations and the stress-strain behaviour of these crystals, the mobility, the multiplication and the interaction of dislocations are investigated.

The strengthening mechanisms and the character of resistive forces which control principally the motion of dislocations in the different types of crystals (bcc or fcc) under the different experimental conditions (tension or compression, low or high temperature, irradiated or unirradiated etc.) are discussed.

1. Introduction

The elementary processes of crystal deformation are the glide motion and the multiplication of dislocations. These processes are essentially dynamical and the studies of these are fundamental to an understanding of plastic flow and strengthening mechanisms in a crystal. It is therefore of primary importance to establish experimentally the relation between the dynamical properties of dislocations and the macroscopic stress-strain behaviour in a crystal by carrying out the direct observation of the dynamical behaviour of dislocations under the known stress-strain condition.

There have been many studies in which attempts have been made to understand the macroscopic plastic flow of a crystal in terms of dislocation theory. However, an understanding of the process has been limited by the fact that most studies have been developed on the basis of the static properties of dislocations. It is only in recent years that workers have realized that crystal deformation must be studied on the basis of dynamical properties of dislocations for our understanding to be advanced further.

For simplicity, consider a group of mobile dislocations, all with the same Burgers vector b in a family of parallel slip planes. If we introduce a mean displacement $<dl>$ of the mobile dislocations, the increment of shear strain is

$$\varepsilon = b \cdot N \cdot <dl> \tag{1}$$

where N is the density of mobile dislocations and b is the magnitude of the Burgers vector. Eqn. (1) denotes a fundamental relation between the mean displacement of dislocations and the macroscopic strain of the crystal. If we introduce the mean velocity $<v>$ of dislocations, the rate of shear strain is given by

$$\dot{\varepsilon} = b \cdot N \cdot <v> \tag{2}$$

Eqn. (2) denotes a fundamental relation by which the movement of dislocations is connected with the macroscopic strain rate.

Johnston and Gilman[1] succeeded in 1959 in deducing theoretically the stress-strain curve in LiF by measuring the velocity of dislocations as a function of stress and the density of dislocations as a function of strain with the aid of a dislocation etching technique. Since then, studies of the dynamical properties of dislocations have been carried out on various crystals by many investigators utilizing various methods, *e. g.*, Stein and Low[2] by dislocation etching, Suzuki and Kojima[3] by X-ray topography and Imura and Saka[4] by electron microscopy. The directest method among them, however, is the method developed by the authors' group, which is based on high voltage electron microscopy (hereafter denoted by HVEM).

The techniques which make use of dislocation etching and X-ray topography are low in resolution and they are not capable of detecting the fast-moving individual dislocations. Therefore, they allow only the comparison of dislocation configurations or the micro slip-bands before and after the application of a stress pulse with known amplitude and duration. Consequently, the motion of individual dislocations cannot be followed continuously by these techniques and the experiments based on these techniques cannot provide detailed information on the elementary processes of dislocation motions in a crystal.

Transmission electron microscopy (TEM) is the only technique currently available for a continuous observation of dislocation motions. However, most of the *in-situ* deformation experiments carried out so far cannot provide actual information on the dynamical properties of dislocations from the following aspects.

1) Where a conventional 100kV microscope is used, the usable specimen is usually too thin to reveal the dynamic behaviour of dislocations in the bulk material.

2) The behaviour of dislocations is not correlated with the stress-strain curve of the specimen being stretched under observation, because the tensile devices are not equipped with load cells.

3) The motion of dislocations is recorded intermittently on the successive ordinary plates, so that it is impossible to record continuously the images of fast-moving dislocations.

4) Where a cine camera is used for a continuous recording, a strong incident beam is needed to record the images even at the frame speed as low as only several frames per second. As a result, the heavy dose of high-energy electrons causes specimen damage by inducing heat and/or contamination.

Since the development of HVEM, the maximum usable thickness of the specimen has been remarkably increased.[5] This advantage of HVEM affords the prospect of observing the same phenomena in specimens as in the bulk materials by a suitable treatment of the specimen in a HVEM. However, in order to realize the same phenomena as in bulk specimens, the specimen foils must be thicker than a certain value which depends strongly on the kind of materials and also the kind of phenomena.[6]

Fig. 1 indicates the maximum usable thickness of specimens against the accelerating voltage of EM, together with the values above which the observed phenomena can be considered as representing the bulk properties for several kinds of specimens and phenomena (indicated by broken lines). For instance, in order to observe the same dislocation behaviour as in the bulk iron crystal, Fig. 1 indicates that (1) a specimen thicker than 1.5 μm must be used and that (2) use of a HVEM operated at an accelerating voltage higher than 500kV is required.

The use of a thicker specimen also implies that each micrograph yields more

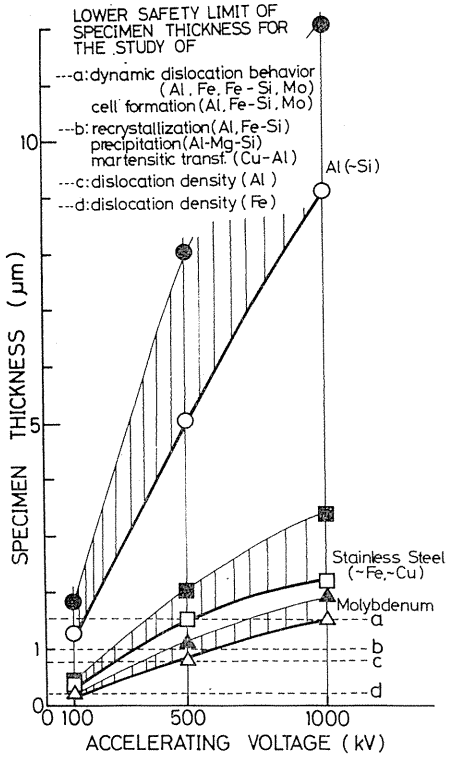

Fig. 1. Maximum usable thickness of the specimen (△, □ and ○) versus accelerating voltage and the lower safety limit of the specimen thickness (broken lines) for the study of (a) dynamical dislocation behaviour (Al, Fe, Fe-3%Si), cell formation (Al, Fe); (b) recrystallization (Al, Fe-3% Si), precipitation (Al-Mg-Si), martensitic transformation (Cu-Al); (c) dislocation density (Al); (d) dislocation density (Fe). The marks, ▲, ■ and ● denote the largest values obtained so far with stainless steel, molybdenum, and aluminum, respectively.

information and that a larger volume of the specimen can be investigated, both factors improving statistics. Hence, HVEM is much more suitable for quantitative metallographic observations than a conventional 100kV level microscope.

Based on HVEM, a new direct method has been developed by the authors' group. In this method, a foil specimen thicker than the aforementioned values (cf. Fig. 1) is stretched while under observation in a HVEM, and the behaviour of individual dislocations in the stressed crystal is recorded continuously by using TV camera and a video tape recorder (VTR). In parallel with the record of dislocation motion, the load-elongation curve of the specimen being stretched is also recorded simultaneouly. Thus, one-to-one correspondence is established between the dynamic behaviour of the individual dislocations observed in a HVEM and the stress-strain condition of the specimen.

The present study is planned primarily to establish a direct correlation between the dynamical properties of dislocations and the stress-strain behaviour in a crystal by observing directly the dynamical behaviour of individual dislocations in some bcc and fcc metals under known tension or alternating tension-compression at various temperatures by means of the *in-situ* deformation experiments in a HVEM.

The aim of the study is, of course, to clarify the strengthening mechanisms and the character of resistive forces which control principally the motion of dislocations in these different types of crystals on the basis of the dynamical properties of dislocations obtained by the experiment.

2. Experimental Procedures

2. 1. Outline of Experimental Procedures

In this experiment foil specimens are deformed plastically in a HVEM in the temperature range from −150℃ to 850℃ ; the behaviour of individual dislocations is observed and recorded continuously and analysed frame by frame to obtain information on the dynamical properties of dislocations.

First of all, specimens much thicker than the aforementioned values (cf. Fig. 1) are used: The observed behaviour of dislocations in such thick foil specimens can be considered to be representative of the behaviour in bulk crystals.

Secondly, the stress-strain curve of the specimen being stretched in a HVEM is recorded in parallel with the record of the images of moving dislocations in the specimen and thus, the one-to-one correspondence is established between the dynamical behaviour of individual dislocations observed in HVEM and the macroscopic stress-strain behaviour of the specimen such as yielding and work-hardening etc. To make this possible, it is necessary to stretch the specimen of a simple shape in outward and cross-section with a tensile device which allows the record of the load-displacement curve of the specimen. Only by using such a simple-shaped specimen it is made possible to calculate the stress-strain curve without ambiguity from the load-displacement curve.

Thirdly, a TV-VTR system is employed for the first time to record continuously the electron microscope (EM) images of fast-moving dislocations.

In the following sections the experimental procedures are described in some detail.

2. 2. Straining Devices

The tensile devices used for *in-situ* deformation experiments in an EM are required to have the following functions.

1) The load-displacement curve can be recorded; a tensile test in a usual sense of the mechanical engineering can be made inside an EM. The stress-strain curve can be calculated from the load-displacement curve in the case where a simple-shaped specimen is used as the tensile test piece.

2) A very smooth and easily controlled straining mechanism allows a continuous recording of dislocation motions while increasing or decreasing the stress and the strain.

3) The devices can be set in a universal tilting goniometer stage. This facilitates the adjustment of Bragg condition which occasionally changes during an *in-situ* deformation. In addition, in order to carry out a contrast experiment or to take stereo-pairs tilting of the specimen is necessary.

4) Specimens can be deformed in a wide range of temperature. The plasticity of metals and alloys is in many cases highly temperature-sensitive. Therefore, a thorough understanding of plastic deformation of metallic materials necessitates to have a knowledge on the dynamical properties of dislocations not only at room temperature but also at lower and higher temperatures.

Various types of tensile device have been developed in order to satisfy these requirements. In the following some typical tensile devices are described in detail and other are mentioned only briefly.

2. 2. 1. Thermal expansion type (for room-temperature deformation)[7]

Fig. 2 (a) and (b) shows the whole view and a schematic illustration of the device, respectively. The device is composed of three parts; one for straining the specimen, one for measuring the applied load and one for measuring the displacement of the movable jaw.

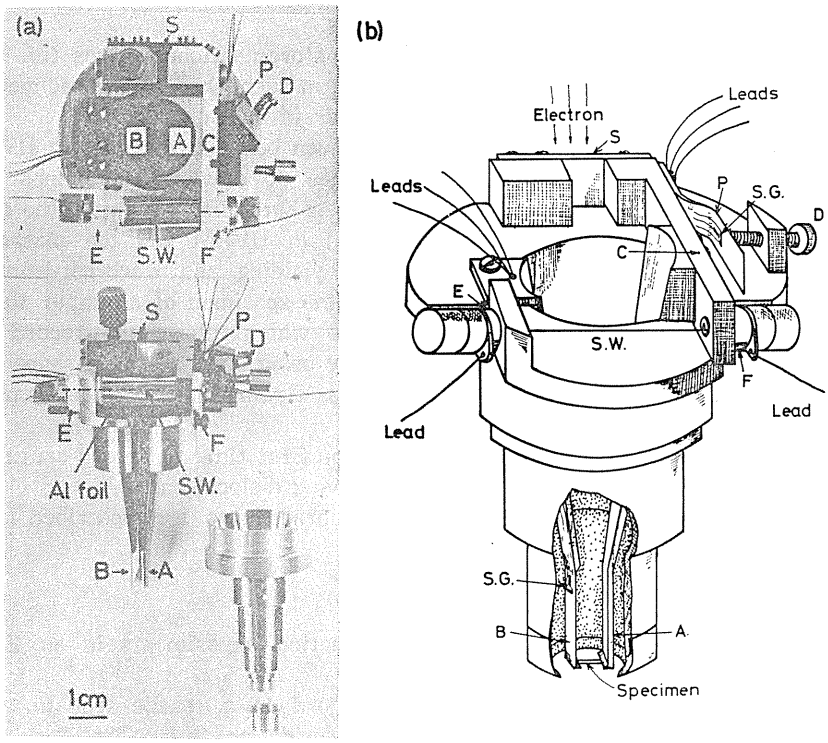

Fig. 2. (a) Whole view of the device using thermal expansion of a heated stainless steel wire.
(b) Schematic illustration.

Straining system

The straining mechanism is in principle similar to that of JEM type.[8] A driving spring S is balanced by the line tension of a stainless steel wire S. W. of about 0.2 mm in diameter. On heating S. W. with direct electric current, the movable jaw A is displaced by an increment in length of S. W. due to thermal expansion and/or deformation. Since the other jaw B is fixed to the stage, the specimen mounted to the two jaws with drops of a strong adhesive is stretched. Because no mechanical linkage is involved in the action of the jaw A, a highly smooth stretching of the specimen is attained.

Measurement of the applied load

The fixed jaw B has a thinned end (0.5 mm in thickness, 10 mm in length), to which high-sensitivity semiconductor strain gauges TENPAC (sensitivity; max., 10^{-8} cm/cm, guaranteed 10^{-6} cm/cm) of Toyota Research and Development Lab. Inc. are

glued as illustrated in Fig. 2 (b). On loading, the jaw A is displaced rigidly, while B is bent elastically in an amount corresponding to the force applied to the specimen; B plays a role of the load cell of a usual tensile testing machine. By calibrating the load cell, the load applied to the specimen can be measured. An example of calibration curve is reproduced in Fig. 3. With this load cell measurements of load from 0.1 gr up to 50 gr are possible and the linearity is exceedingly good. Needless to say, the sensitivity is much improved if use is made of a thinner plate as B. For example, by using a plate of 0.12 mm in thickness, the minimum increment of the load to be detected is as small as 0.01 gr.

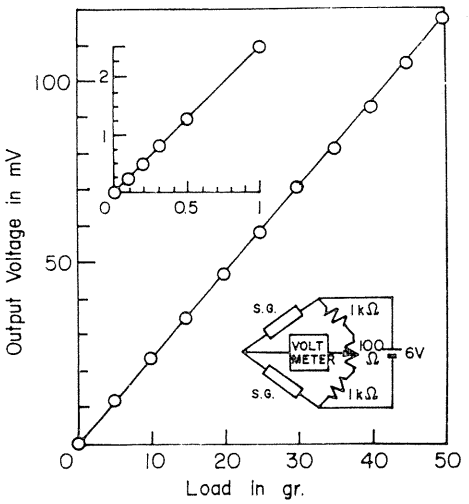

Fig. 3. Example of calibration curve of the load cell.

Measurement of the displacement of movable jaw A

The semiconductor strain gauges are glued on a thin plate P attached to an arm C to which the movable jaw A is in turn fixed. Initially the plate P is bent slightly by an adjusting screw D (cf. Fig. 2). On heating S. W., the arm C is displaced together with the movable jaw A by the action of the elastic force of the spring S, and P is bent elastically in an amount corresponding to the displacement of C and hence A. The calibration curve of the displacement of A versus output signals from the strain gauges is similar to that for the load cell B (Fig. 3).

Load-displacement curve

The output signal from a set of the strain gauges which are used to measure the applied load is fed into the Y-axis and that from the other set measuring the displacement of the movable jaw A into the X-axis of an X-Y recorder; thus, the load-displacement curve is recorded automatically. An example of such load-displacement curve is reproduced in Fig. 4. Various stages of deformation such as elastic region, yield point, work-hardening region and fracture, all of which characterize macroscopic features of the deformation, can be easily identified along the load-displacement curve illustrated in Fig. 4.

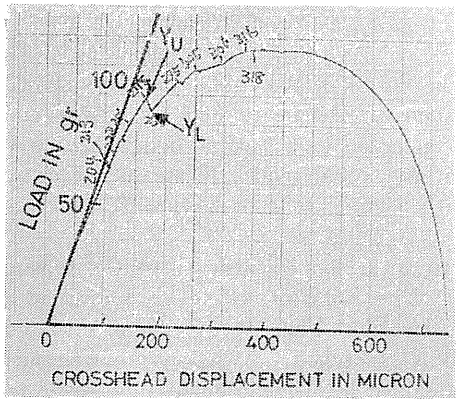

Fig. 4. Example of load-displacement curve of the foil specimen stretched in HVEM. The numbers on the curve indicate those of tape counter of VTR.

This device is the first one in the world to detect the load-displacement curve of the specimen being stretched while under observation in an EM.

2. 2. 2. Cable release type (from −150℃ to 150℃)[9]

Instead of using thermal expansion of a heated stainless steel wire as a straining mechanism, quite a novel straining mechanism is devised by making use of a modified cable release for a camera shutter. Figs. 5 and 6 show a schematic illustration and

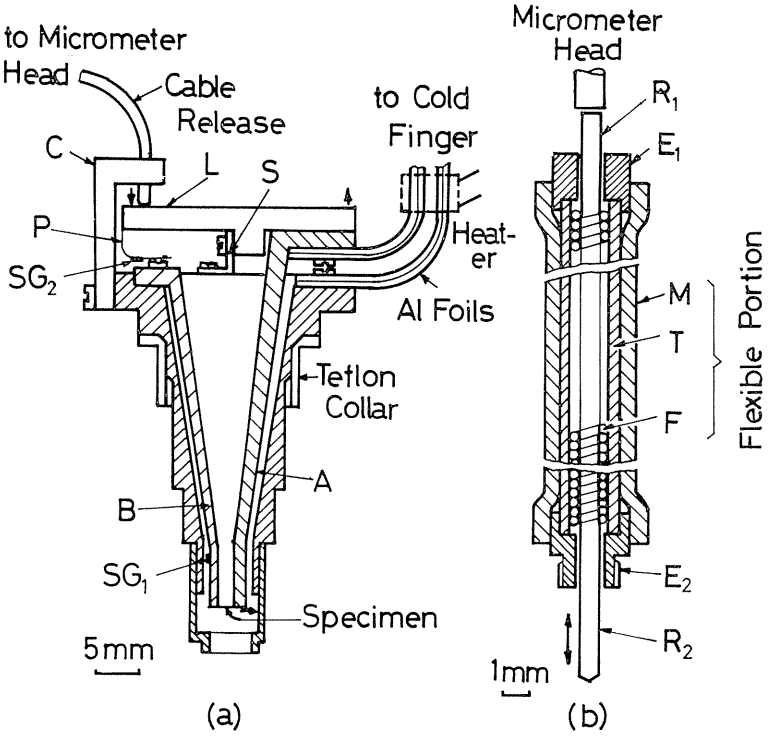

Fig. 5. (a) Schematic illustration of the tensile device using a cable release.
(b) Details of the cable release.

the whole view of the device, respectively. The detail of the cable release is shown in Fig. 5 (b). The release is fixed to the column of EM at its end E_1. The rod R_1 is driven with a micrometer head. R_1 is connected to a flexible helical spring F which is in turn connected to a push rod R_2 at the other end. F is displaced by the motion of R_1, keeping a close contact with a guide tube of Teflon T, which is reinforced by a metallic mesh M.

The other end of the release E_2 is fixed to an L-shaped arm C of the tensile device and the rod R_2 pushes the lever L. The rotation of lever L around a fulcrum spring S displaces the movable jaw A outwards. Thus, the specimen mounted across the movable jaw A and the fixed jaw B is stretched. A highly smooth and easily controlled motion of the jaw A is attained by using a guide tube made of Teflon instead of a guide of a helical spring used in a commercial cable release. In addition, a nearly constant strain rate is achieved by driving the micrometer head with an electric motor. To change the strain rate as well as to stop straining or to change the direction of straining is also easily made.

This device can be used in the temperature range from −150℃ to 150℃. Cooling of specimen is actuated by connecting the device with Al foils to a cold trap which is cooled by liquid nitrogen. Heating of the specimen up to 150℃ is made with a small heater attached to the Al foils. Flexibility of the cable release and the Al foils makes it possible to set the device in a usual goniometer stage.

Measurements of the load applied to the specimen and also the displacement of the movable jaw A are made in a way similar to that used in the tensile device described in Sec. 2. 2. 1. The semiconductor strain gauges can be used effectively from −150℃ to 150℃.

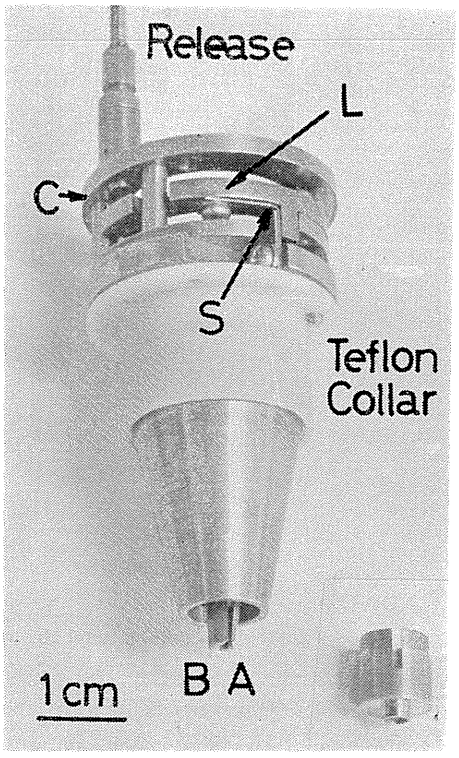

Fig. 6. Whole view of the device sketched in Fig. 5.

2. 2. 3. *High-temperature tensile device (from room-temperature to* 850℃)[10]

Although the aforementioned tensile device can be used from −150℃ to 150℃, an experiment at still higher temperatures is often required. For such an *in-situ* deformation experiment at a high temperature a tensile device usable from room temperature to 850℃ has been developed (Fig. 7). A small furnace is attached to the fixed jaw of the device to heat up the specimen. The furnace is made of non-inducingly wound coil of tungsten. The main body of the device is connected to the furnace only through a thin wall made of austenitic stainless steel (18/8) to prevent the heat conduction. Temperatures are measured with copper-constantan thermocouples at the three points of the device as follows. (1) The fixed jaw to which the furnace is attached (approximately the temperature of the specimen is measured.). (2) The strain gauges to measure the load. (3) The strain gauges to measure the displacement of the movable jaw A. Not only the temperature of specimen but also the temperatures of the strain gauges are controlled throughout an experiment and the temperatures of these strain gauges are suppressed below 200℃. This is because the strain gauges cannot be used above 200℃.

The straining mechanism as well as the method of measuring the load-displacement curve is the same as that used in the aforementioned devices.

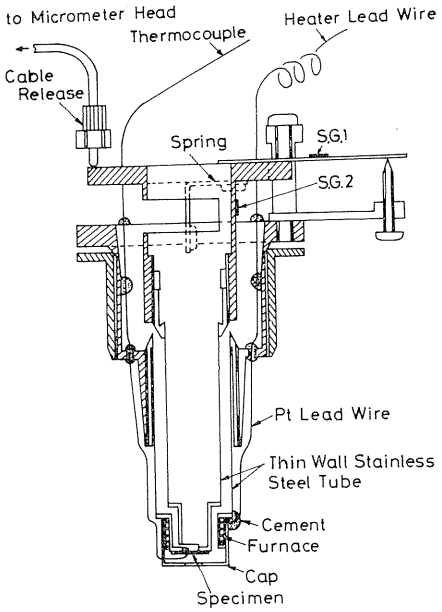

Fig. 7. A cross-sectional drawing of high-temperature tensile device.

2. 2. 4. Other types of tensile device

Employing straining mechanisms other than the aforementioned two types, two types of straining device with similar functions have been developed, which are described briefly in the following. In these, the method to detect the load-displacement curve is the same as that used in the aforementioned devices.

In one of these, hydrostatic pressure of oil in a closed system is used to drive the lever to which the movable jaw is attached (similar to the lever L in Fig. 5)[11]. In the other[12], a small pulse-motor is built in the device and is used to drive the movable jaw. The motor is electrically shielded to avoid the disturbance of electron beam. These two tensile devices allow the deformation of a specimen at constant strain rates, provided that the specimen has a cross-section which is uniform along its gauge length. These tensile devices can operate at room temperature.

2. 2. 5. Push-pull straining device[13]

The plasticity of metals and alloys when they are deformed alternately in tension and compression is quite different from that when deformed uniaxially. Such a behaviour of materials under an alternate stress is closely connected with the so-called Bauschinger effect and also the fatigue process of materials. These phenomena are of theoretical as well as practical importance. In order to observe the dynamical behaviour of individual dislocations under alternate stresses, a push-pull straining device for an *in-situ* deformation experiment in HVEM has been developed.

Fig. 8 (a) and (b) shows a schematic illustration and the whole view of the device, respectively. A foil specimen is glued onto a substrate plate S made of Cu-Be. One end of S is fixed to the outer shell of the device O and the other is

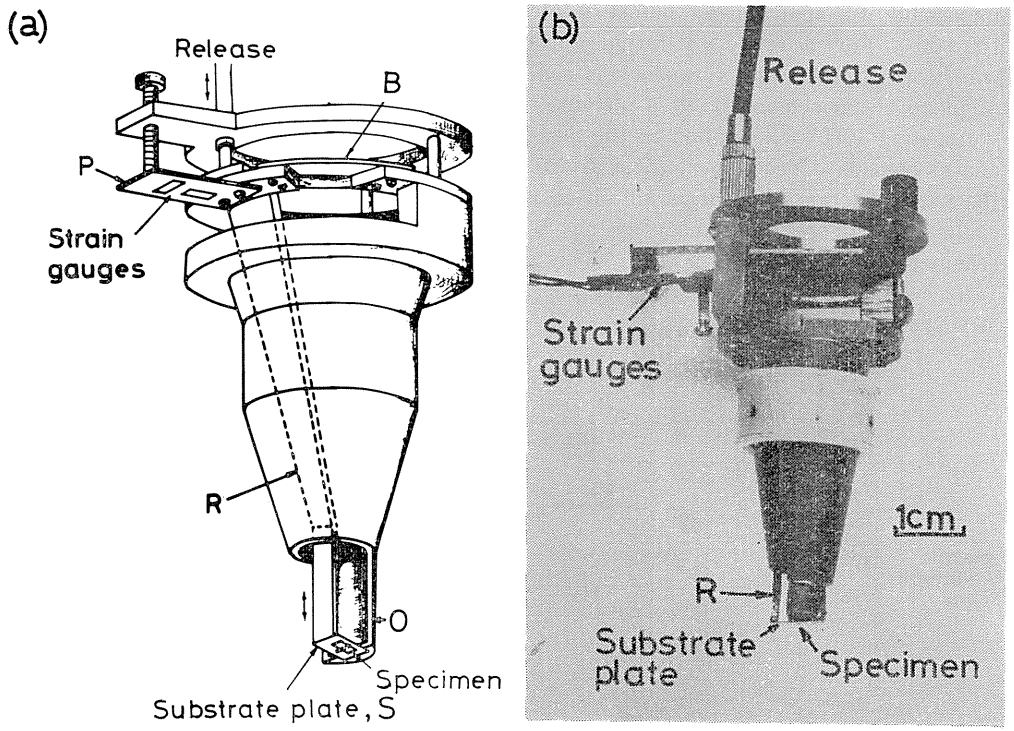

Fig. 8. (a) Schematic illustration of push-pull straining device.
(b) Whole view of the device.

fixed to one end of the movable rod R. The other end of R is fixed to a fulcrum spring B. The rod R is displaced up and down by the action of a cable release, and S is bent alternately. Since the thickness of S is much larger (0.1 - 0.2 mm) than that of foil specimens (max., a few microns), the foil specimen glued onto S is compressed or stretched, depending on the sense of bending of S, as is schematically shown in Fig. 9. There is a narrow slit at the center of S and the specimen bridging the slit is examined by transmission electron microscopy.

The displacement of the movable end of S is measured with high sensitivity semiconductor strain gauges glued on a thin plate P which is attached to B. Thus, the strain applied to the specimen is measured and controlled.

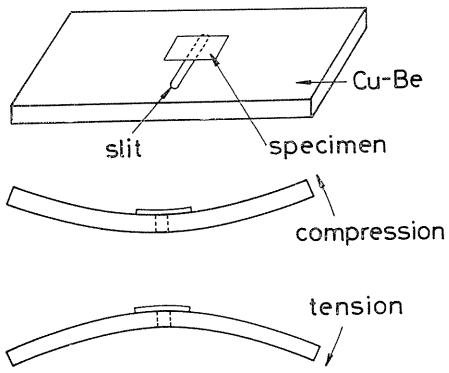

Fig .9. Principle to apply push-pull strain to the foil specimen.

2. 2. 6. *In-situ fatigue device*[14]

Although the aforementioned push-pull straining device is convenient to apply a few numbers of alternate stress cycles to the specimen, it is in practice

impossible to apply many numbers of alternate stress cycles such as 10,000 or 100,000. For a study of fatigue process of metals an alternate-stressing device which operates at high frequency is required. This can be achieved by making use of piezo electric element as a driving force of stressing, Fig. 10. An alternate voltage (± 1000V) is applied to the piezo electric element P, which repeats shrinkage and elongation depending on the sign of the applied voltage. The change in length of the piezo electric element is amplified by a lever L and a substrate plate S is bent cyclically. A specimen mounted on S is subjected to push-pull stress cycles as schematically shown in Fig. 11. This device operates at a frequency ranging from 1 Hz to 1000 Hz and *in-situ* fatigue test on foil specimens can be made during observation in HVEM.

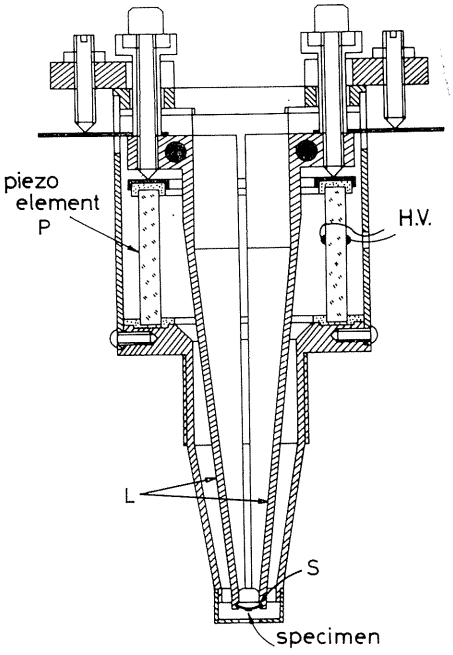

Fig. 10. Schematic illustration of *in-situ* fatigue device.

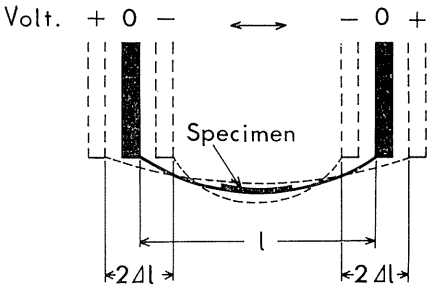

Fig. 11. Curved specimen mounted across the two jaws is subjected to a push-pull strain, as the separation between the two jaws repeats an increase-decrease cycle.

2. 3. Tensile Test Pieces for In-Situ Deformation Experiments in HVEM.

2. 3. 1. Introduction

The stress and the strain applied to the area of specimen just being examined in HVEM are calculated from the recorded load-displacement curve by dividing, respectively, the load by the cross-sectional area and the displacement of movable jaw by the initial length of the specimen. In this method, it is assumed that there is no strong irregularity in shape which leads to a stress concentration and a local deformation of the specimen. Therefore, it is desirable that the specimens used for *in-situ* deformation experiments have simple shapes similar to those used in a conventional tensile test.

Another practical difficulty in an *in-situ* deformation experiment is the attach-

ment of the specimen to the jaws of the tensile device: The specimen must be mounted to the tensile device without strain being introduced.

This section describes the experimental procedures of preparing the micro-tensile test pieces for *in-situ* deformation experiments and for mounting the specimens to the jaws of the tensile devices without introducing strain. Emphasis should be on that whether or not an *in-situ* deformation experiment can be carried out successfully does rely strongly on the techniques of preparing and mounting the specimens.

2. 3. 2. *Preparation of tensile test pieces from bulk crystal by electro-polishing*

Although plate-like whiskers prepared by vapour deposition have been used as tensile test pieces for *in-situ* deformation experiments in EM by some investigators[15~17], growth of such plate-like whiskers cannot be applied universally to all metals and alloys and for this reason this technique has been applied successfully only to zinc[15, 17] and cadmium[16] so far*. Electro-polishing on the other hand, can be applied almost to all metals and alloys.

As a tensile test piece for an *in-situ* deformation experiment in an EM the specimen as indicated in Fig. 12 (a), which is originally due to Wilsdorf[19], has been exclusively used so far, since the preparation of such a specimen is relatively easy.[20)~23)] In this case, observation is confined to the thin region around the hole. This type of specimen, however, has a serious disadvantage that the stress concentration around the hole is large and that the stress and the strain are too complicated to be analysed accurately. As a result, it would be meaningless to attempt to estimate the stress and the strain applied to such a specimen by using a stress-strain measuring tensile device described in Sec. 2. 2.

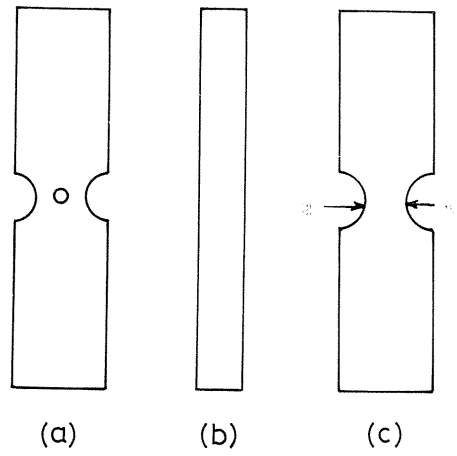

Fig. 12. Specimens for *in-situ* deformation experiment in EM.
(a) This type of specimen is due to Wilsdorf and not used in this study.
(b), (c) These specimens were used in the present *in-situ* deformation experiments to facilitate the measurement of the stress-strain relationship.

The present authors have developed new techniques to prepare the specimens with simple shapes for *in-situ* deformation experiments which facilitate the estimation of stress and strain applied to the area of specimen being observed in EM.

Figure-of-eight method[4)]

This is a modified "figure-of-eight" method and can be applied universally to almost all metals and alloys, provided that a proper elecrolyte is used for the

* Recently some preliminary *in-situ* deformation experiments on the whiskers of copper and iron have been made by using HVEM and SEM[12)].

respective materials. The procedures are as follows. A sample is polished either chemically or mechanically down to the thickness of 0.1 mm. One side of the sample is coated with laquer leaving a window of figure-of-eight as shown in Fig. 13 (a), while the other side is coated as in a usual window method, Fig. 13 (b). Then, the sample is electro-polished. A preferred polishing occurs at the border

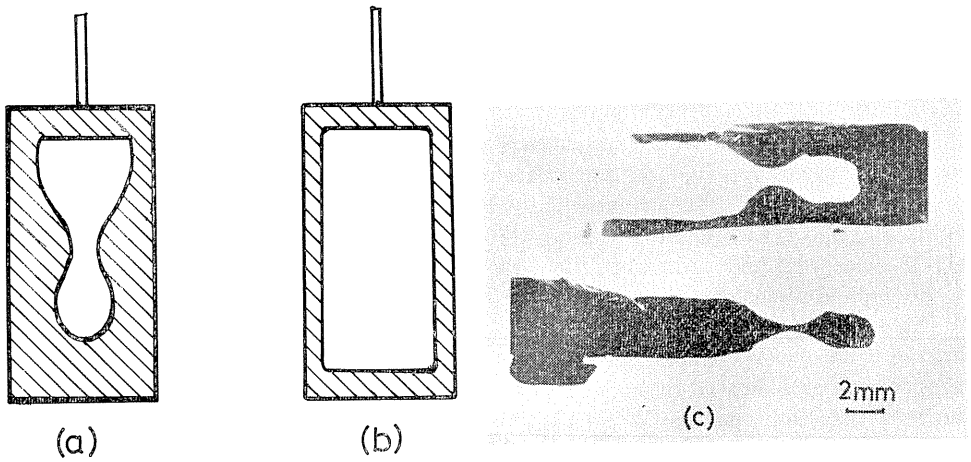

Fig. 13. Modified "figure-of-eight" method.

of the laquer and the specimen, resulting in a perforation of the specimen in a shape of figure-of-eight, as shown in Fig. 13 (c). Instead of coating the sample with laquer, jet polishing can also be used to perforate the sample in figure-of-eight, as shown in Fig. 14.[24]

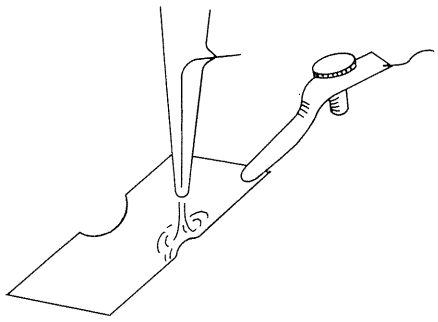

Fig. 14. Jet-polishing technique applied to perforate specimen.

Window method[24]

This is essentially a window method, which can be applied to aluminum. The sample of about 0.1 mm in thickness is laquered to leave a window of $2 \times 2\,cm^2$, followed by polishing with a U-shaped cathode in the solution of 1 vol. of perchloric acid and 3 vol. of methanol at $-30℃$, with an applied voltage and a current density of 15V and 0.1 A/cm^2, respectively. If no stirring of electrolyte is made, bubbles evolving at the lower border between the laquer and the sample creep upwards vertically on the surface of the sample.* The preferred polishing of the sample along the tracks of the bubbles results in a perforation of the sample in a comb-like shape, as is shown in Fig. 15. A tooth having parallel edges is cut from the comb with a razor blade and used as a tensile test piece.

* It is essential to cool the electrolyte by immersing solid CO_2 directly into the electrolyte to enhance the evolution of bubbles.

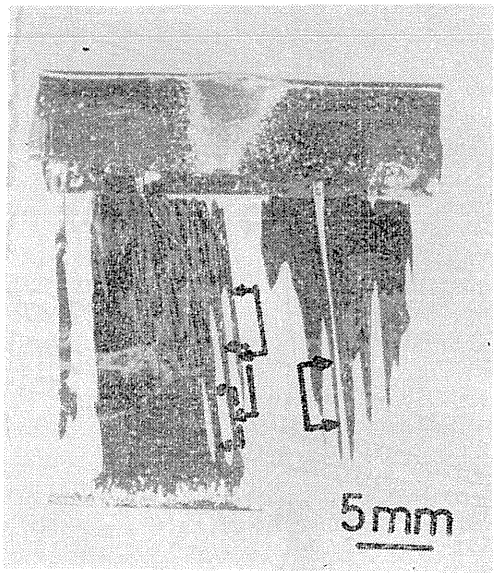

Fig. 15. Comb-like specimen prepared with a window method.

2. 3. 3. Mounting specimen to the tensile device

Mounting the specimen to the jaws of a tensile device without introducing strain is practically as important as preparing a simple-shaped specimen. The following three requirements must be satisfied.

1) The specimen can be attached to the jaws of the tensile device with no strain being introduced. The specimen must not be rumpled when the adhesive is dried. It is also desirable that time for curing the adhesive is short enough.

2) The adhesive must be strong enough to deform the specimen plastically. The total load applied to the specimen often amounts to as large as several hundreds grams, when a strong specimen is used. The adhesive must be effective at low and high temperatures.

3) The specimen must be detached from the jaws with no additional strain being introduced after an *in-situ* deformation experiment. This is required because it is often necessary to examine the specimen after it is deformed in HVEM by optical microscopy and/or scanning electron microscopy in order to carry out a trace analysis of the slip lines appearing on the surface of a specimen.

The present authors have established a method for mounting the specimen to the jaws of a tensile device in such a way as to satisfy the aforementioned requirements.[25]

A specimen is picked up by the end with specially designed pincers depicted in Fig. 16. The opening as well as shutting of the jaws of the pincers is actuated by a commercial cable release R for a camera shutter. The jaws of the pincers open when the release is pushed and close when it is relaxed. A backward motion of the jaws is achieved with an elastic rubber E. The specimen as picked by the end with the pincers is attached onto the jaws of a tensile device with drops of a strong adhesive with the aid of a manipulator under examination of a binocular microscope. Prior to *in-situ* deformation it must be confirmed by optical and

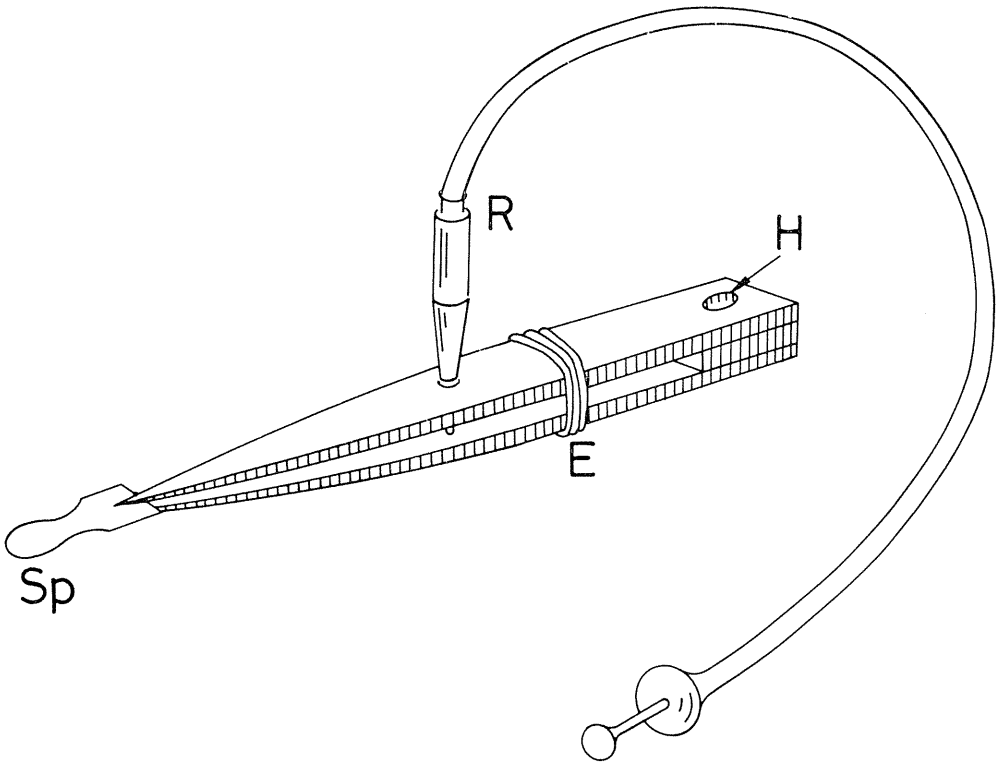

Fig. 16. Specially designed pincers to pick up the specimen,

electron microscopy that no strain is introduced into the specimen by handling.

As far as an adhesive is concerned Armstrong A-36 is effective from -150℃ to room temperature. From room temperature to 180℃ Epikote 828 is effective. These adhesives are dissolved in n, n-dimethylformamide and thus, the specimen can be detached from the jaws of a tensile device after it is stretched *in situ* in HVEM.

For a deformation at higher temperature such as 800℃, these adhesives can no longer be used.* In this case, micro-spot welding technique[26] has been applied successfully. However, detachment of the specimen from the device must be made mechanically.

2. 3. 4. Estimation of stress and strain applied to specimen

The most striking advantage of the present *in-situ* deformation experiment over the conventional ones is that the stress and the strain applied to the specimen are measured. This is done by calculating the stress and the strain from the recorded load-displacement curve through a knowledge of the dimension and shape of the specimen used. In this section, the procedures for estimating the stress and the strain from a load-displacement curve are described.

A specimen is detached from the jaws of a tensile device after it is stretched

* (*note added in proof*) : Recently it is shown that CERAMABOND 512 of Aremco Co. Ltd. is effective up to 1000℃.[77]

in situ in HVEM and cemented in epoxy resin. Then it is cut with a razor blade along the deformed region where the behaviour of dislocations was observed. The section is examined with an optical microscope to measure the cross-sectional area. The tensile stress is thus calculated by dividing the load by the cross-sectional area. The overall elongation is determined by dividing the increment in separation between the two jaws of the tensile device by the initial separation.

Two types of specimen are used in the present *in-situ* deformation experiments. They are shown schematically in Fig. 12 (b) and (c). The specimen shown in Fig. 12 (b) has parallel edges and a relatively uniform cross-section along its gauge length. Such a specimen deforms homogeneously over the gauge length except in the vicinity of the jaws. That is, there is only a negligibly small variation in stress and strain along its gauge length at least to the first approximation. Thus, the overall stress-strain curve obtained on such a specimen in the aforementioned manner must coincide with the local stress-strain curve of the region of specimen being observed in HVEM.

In the case of the specimen depicted in Fig. 12(c), situations are rather complicated, since it has neither parallel edges nor uniform cross-section along its gauge length. The overall elongation of the specimen can be measured in the manner described above but the local elongation of the narrowest region of specimen observed in EM would be larger than the overall elongation, since deformation takes place preferentially in this region*. Thus, the strain obtained in the aforemeotioned manner for a specimen of this type must be taken as providing only a measure of the true strain.

The specimen shown in Fig. 12 (b) has no stress concentration anywhere along its gauge length. The specimen shown in Fig. 12 (c) has a stress concentration factor ranging from 1.1 to 1.2 but an error arising from this stress concentration in estimating the stress is only a minor one as compared with the case of specimen shown in Fig. 12 (a) which has a stress concentration factor of as large as 3 in the vicinity of the hole.

Another problem is due to the fact that the cross-sectional profile of the specimen is not rectangular but lenticular (cf. Fig. 17). If a thin crystal in the

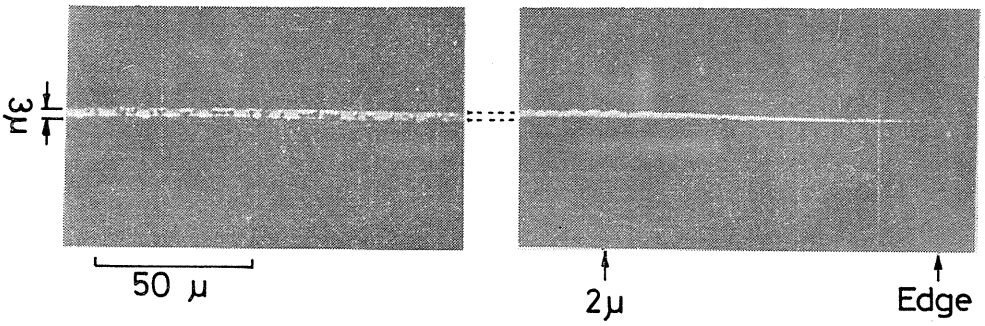

Fig. 17. An example of cross-sectional profile of the specimen used in this study.

* This is practically convenient to observe the motion of dislocations especially at an early stage of deformation.

near-edge region of specimen is either harder or softer than a thicker crystal in the central region of specimen, there is no one-to-one correspondence between the observed behaviour of dislocations and the recorded stress-strain curve, because the observation is made in the thin near-edge region of specimen, while the recorded stress-strain curve is concerned mostly with the thicker central region of specimen and the stress-strain relationships for both regions are not identical in such a case. However, this possibility is ruled out from the following considerations.

The slip lines appearing on the surface of a foil specimen are distributed uniformly across the width of specimen even at an early stage of deformation. Thus, the plastic strain of the near-edge region of foil is identical to that of central region. This is confirmed by direct observations of the dislocation motions in foil specimens being stretched in HVEM. The motion of dislocations becomes active as the yield point is reached. The observed activity of dislocation motions and the recorded yield point coincide exactly one with other. Thus, it is reasonable to conclude that the stress-strain relationship of the near-edge region of foil is identical to that of central region of specimen at least at an early stage of hardening, unless a sophistical assumption is made that the elastic constants are substantially different for both regions. Thus, the one-to-one correspondence is established between the observed behaviour of individual dislocations and the recorded stress-strain curve.

2. 4. Video Recording of Electron Microscope Images of Moving Dislocations

2. 4. 1. Introduction

For recording dynamical phenomena occurring in a foil specimen cine photography has been used so far.[27] There are two arrangements. The first one is simply to photograph EM images produced on a tilted fluorescent screen through the viewing window. The greatest disadvantage of this method is that the maximum frame speed is as low as about 10 frames/sec., even if a wide aperture lens and a high sensitivity cine film are used under a very strong illumination of electron beam. The other technique is to use a specially designed camera which fits into a port of the microscope. The chief disadvantage of this technique is that the actual area being recorded cannot be viewed. As a result, the selection of the area being recorded and the magnification as well as the adjustment of focus, illumination and Bragg condition etc. cannot be made during recording; it is very difficult in practice to record successfully the dynamical phenomena occuring in a foil specimen.

The present authors have applied a modern televison and video recording technique for recording the EM images of moving dislocations[4,18]. In this section this technique of televising and recording the EM images is described.

2. 4. 2. General assembly

A block diagram of the recording system is shown in Fig. 18. EM images are converted by a TV camera into video signals and recorded continuously on a video tape. The recorded motions of dislocations are analysed frame by frame by playing back VTR at the normal speed (30 frames/sec.) and / or a slower speed. In many cases the TV images reproduced from VTR are photographed with a synchronized cine camera on a movie film and analysed frame by frame. The reason of this is that the picture quality of TV images reproduced at a slow speed from VTR is too

poor for detailed configurations of dislocations to be resolved.

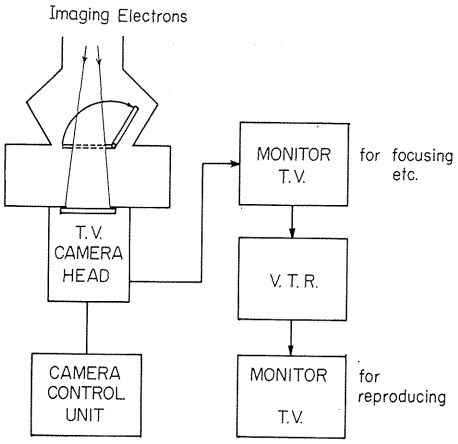

Fig. 18. Block diagram of TV-VTR recording system.

2. 4. 3. Details of TV camera

There are two methods to televise EM images. The arrangements are schematically shown in Fig. 19. The first one (direct method), Fig. 19 (a), is to convert directly the imaging electrons into video signals with an open vidicon-tube equipped with a target exhibiting an electron-bombardment-induced conductivity (EBIC).[28,29] The main disadvantages of this type (particularly in the case of amorphous Se target) are as follows.

1) The efficiency of image intensification is low.
2) Life time of the vidicon as well as the target is very short.
3) Operation is rather complicated.

For these reasons this type of TV camera was used only in the preliminary

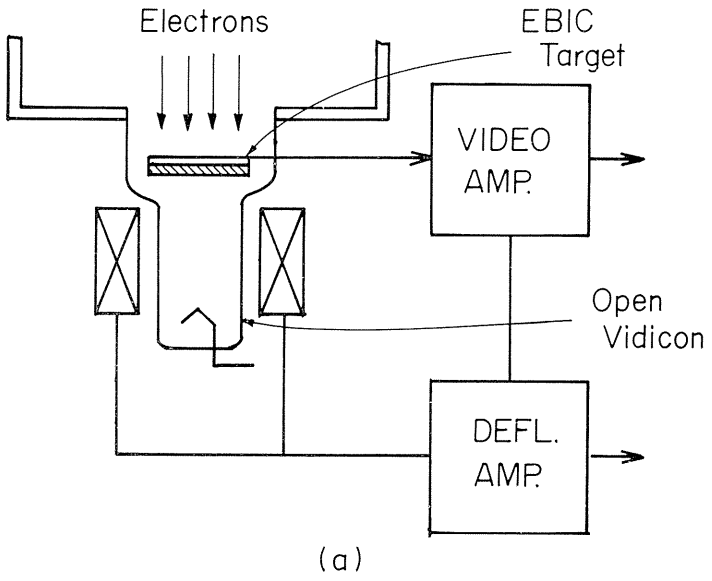

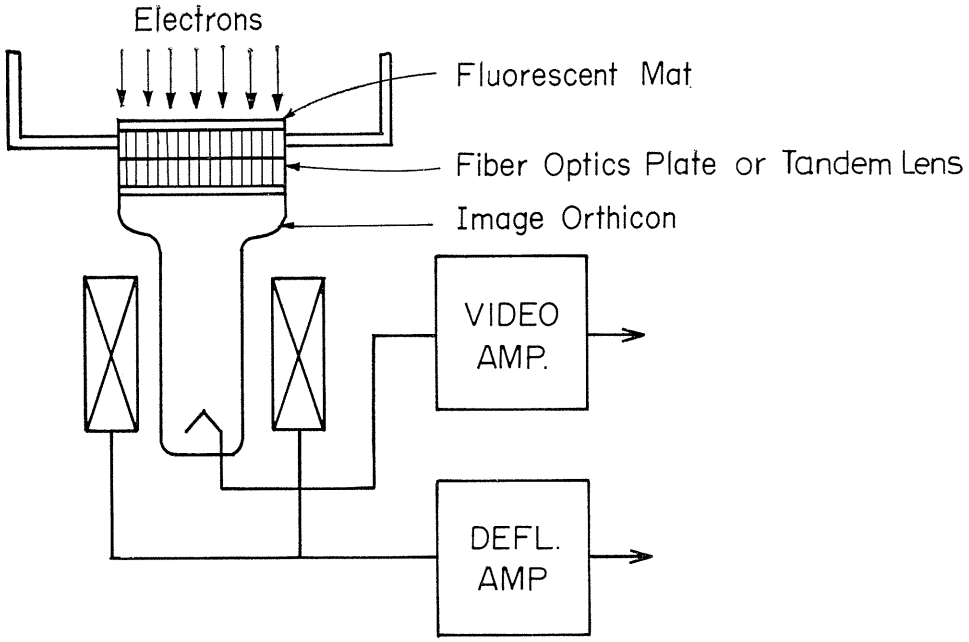

(b)

Fig. 19. (a) Direct method to televise EM images.
(b) Indirect method.

course of the present study.

The other method (indirect method), Fig. 19 (b), is to view with a conventional high-sensitivity TV camera those light images which are formed on a transmission phosphor plate by the imaging electrons. Either a fiber-optics plate or a high-speed tandem lens is used to transfer the light images to the photocathode of the TV camera with only a minor loss in brightness.

Various types of TV camera of indirect method can be constructed by choosing an appropriate combination of the image pick-up tube and the light-transferring

Table 1. Comparison of TV cameras of indirect method.

	Tube	Target	Light Transfer	Merits	Demerits
1.	SEC Vidicon	KCl	Tandem lens or Fiber optics plate	High sensitivity and relatively low lag	Poor resolution
2.	Image Orthicon	MgO	Tandem lens	High sensitivity and low lag	
3.	Fiber plate Image Orthicon	MgO	Fiber optics plate	Sensitivity is higher than (2) Low lag	
4.	EBS	Si diode array	Tandem lens	Extremely high sensitivity	Relatively large lag.

system. Table 1 shows some examples of the combination, together with the merits and demerits of the respective systems. A proper choice of the system is required, depending on the purpose of the experiments. With a proper combination an observation at a very low illumination is possible.

As an example, Fig. 20 shows photographs of the dislocation images in MoS_2 as observed with a TV camera using a fiber-optics plate and a 3 inch image orthicon

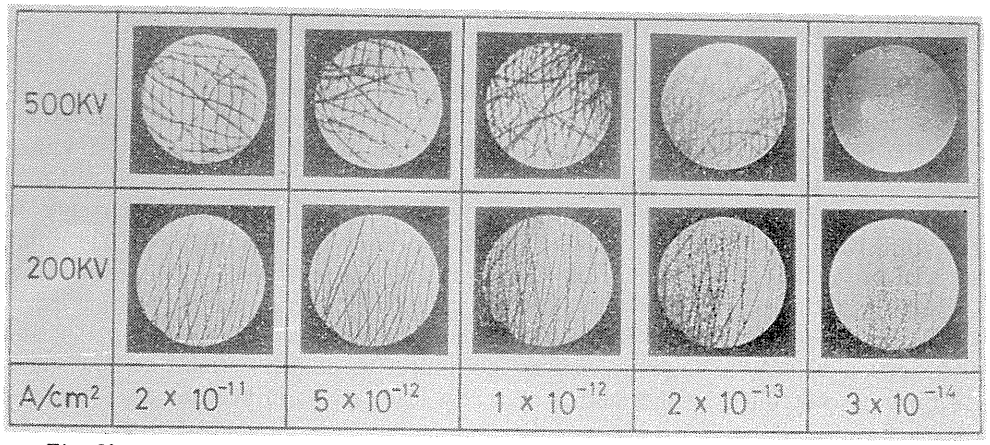

Fig. 20. Examples of observation of dislocation images in MoS_2 with a TV camera using fiber-optics plate and 3 inch image orthicon tube.

tube (HS-191 made by Hitachi Electronics Co. Ltd., MgO target)[30]. The abscissa indicates the electron density (measured with a Faraday cage). Dislocation images can be observed even at an illumination level of 3×10^{-14} A/cm^2 both at 200kV and 500kV, although the efficiency of the fluorescent materials is reduced with increasing the energy of electrons.

2. 4. 4. Summary

To summarize, the main advantages of the recording technique using TV-VTR system over a conventional cine photography are as follows.

1) High frame speed (60 fields/sec., 30 frames/sec.) is obtainable. The corresponding upper limit of velocity which can be measured with this frame speed is an order of 10^{-2} cm/sec. in the case of magnification of 10,000 times.

2) A low illumination observation is possible and this may suppress the damage and the contamination of the specimen due to the bombardment of high energy electrons during observation.

3) Various operations such as focusing, the selection of magnification and the area being recorded and also the adjustment of illumination and Bragg condition etc. are performed easily by viewing a monitor TV. All of these features are essential for a continuous recording of dislocation motions to be performed successfully.

On the other hand, main disadvantage of TV method is that the picture quality is poorer than that of cine photography. Therefore, it is necessary to photograph EM images on ordinary plates in the case where high-resolution micrographs are required for a detailed analysis of dislocation configurations.

3. Elementary Process of Plastic Deformation of BCC Metals at Low Temperatures

3. 1. Introduction

It is well known that the plasticity of bcc metals at low temperatures is very much different from that of fcc metals. [31, 32] The critical resolved shear stress (CRSS) of bcc metals increases much more rapidly with decreasing temperature than that of fcc metals. Furthermore, the geometry of slip and its dependence on temperature and crystal orientation is much more complicated than for fcc metals. *In-situ* deformation experiments on bcc metals in a wide range of temperature provide important information on the dynamical properties of individual dislocations and this facilitates an understanding of the mechanism controlling the plastic flow of bcc metals at low temperatures.

In this chapter the results obtained by the *in-situ* deformation experiments in HVEM on the mobility and the multiplication mechanisms of dislocations in some bcc metals at low, room and high temperatures are described. The controlling mechanism of the plastic flow of bcc metals at low temperatures is discussed in terms of the dynamical properties of individual dislocations. It is shown that the expansion of dislocation loops as well as multiplication of dislocations at low temperatures is controlled by the motion of screw dislocations in bcc metals.

3. 2. Mobility of Edge and Screw Dislocations in Fe, Fe-3%Si and Mo

3. 2. 1. General features of dislocation behaviour in bcc metals at low and high temperatures

The behaviour of individual dislocations in bcc metals at low temperatures is quite different from that at high temperatures. This can be most clearly demonstrated by the *in-situ* deformation experiments which were carried out on Fe and Mo from 150K to 400K. Fig. 21 shows typical configurations of dislocation loops expanding in Mo and Fe foil specimens under the action of the applied stress at the temperatures indicated[33]. Since the melting points of Fe and Mo are substantially different one from other, a homologous temperature should be used in comparing the dislocation behaviour in these materials at different temperatures.

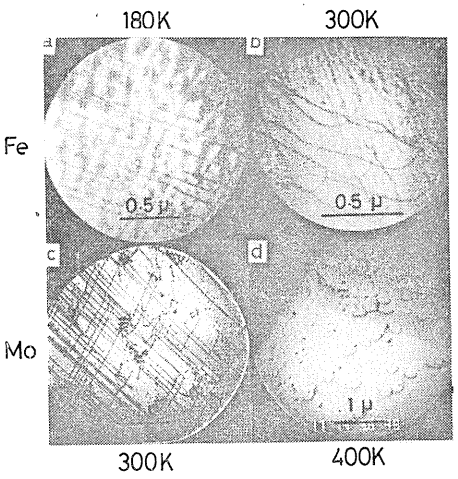

Fig. 21. Configurations of moving dislocations in Fe and Mo at various temperatures.

At low homologous temperatures (*i. e.*, $\leqq 0.1\ T_M$, where T_M is the melting point in Kelvin) dislocation loops are elongated along the direction of Burgers vector $<111>$, while they tend to take circular shapes rather than ellipses with increasing the homologous temperature. This means

that at low temperatures edge components of a dislocation loop move much faster than screws and that at high temperatures the velocity of screw components becomes comparable as that of edge components.

Another difference in the dynamical behaviour between edge and screw dislocations in bcc metals at low temperatures is the difference in flexibility of moving dislocation lines. An example is shown in Fig. 22, which shows the configuration of moving dislocations of edge (non-screw) character and screw character in Fe-3%Si

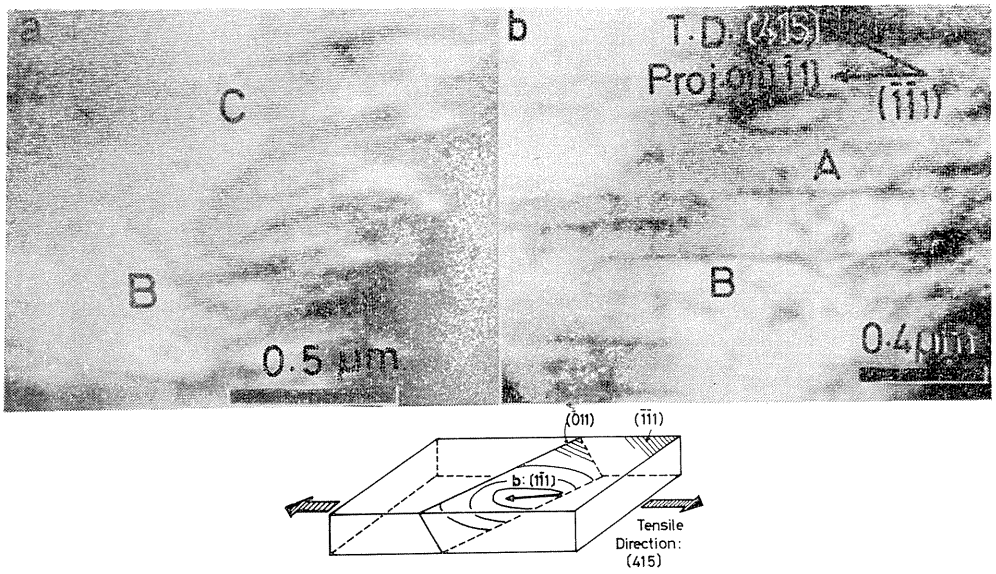

Fig. 22. (a) Behaviour of edge dislocations in Fe-3%Si at room temperature.
(b) Behaviour of screw dislocations in Fe-3%Si at room temperature.

deformed at room temperature (in a low-temperature range for this material)[4]. It can be seen that edge dislocations move like flexible strings but that screw dislocations move keeping the straight shapes. This feature of screw dislocations is in good agreement with the predictions of the current theories that the Peierls potential for a screw dislocation in bcc metals is much higher than that for an edge dislocation. At low temperatures the Peierls potential for a screw dislocation is so high that it is overcome by a screw dislocation only with a double-kink mechanism, resulting in a straight configuration on microscopic scale. On the other hand, an edge dislocation can overcome its Peierls potential easily even at low temperatures, because the Peierls potential is low enough. Same is true for a screw dislocation moving at high temperatures, where the Peierls potential is overcome easily with the aid of thermal energy and renders no longer a strong barrier to the motion of a screw dislocation. As a result, moving screw dislocations behave like flexible strings.

3. 2. 2. *Quantitative determination of velocity of individual dislocations as a function of the applied stress*

In-situ deformation experiment renders a powerful tool for the determination of mobility of individual dislocations of known character (edge and screw).

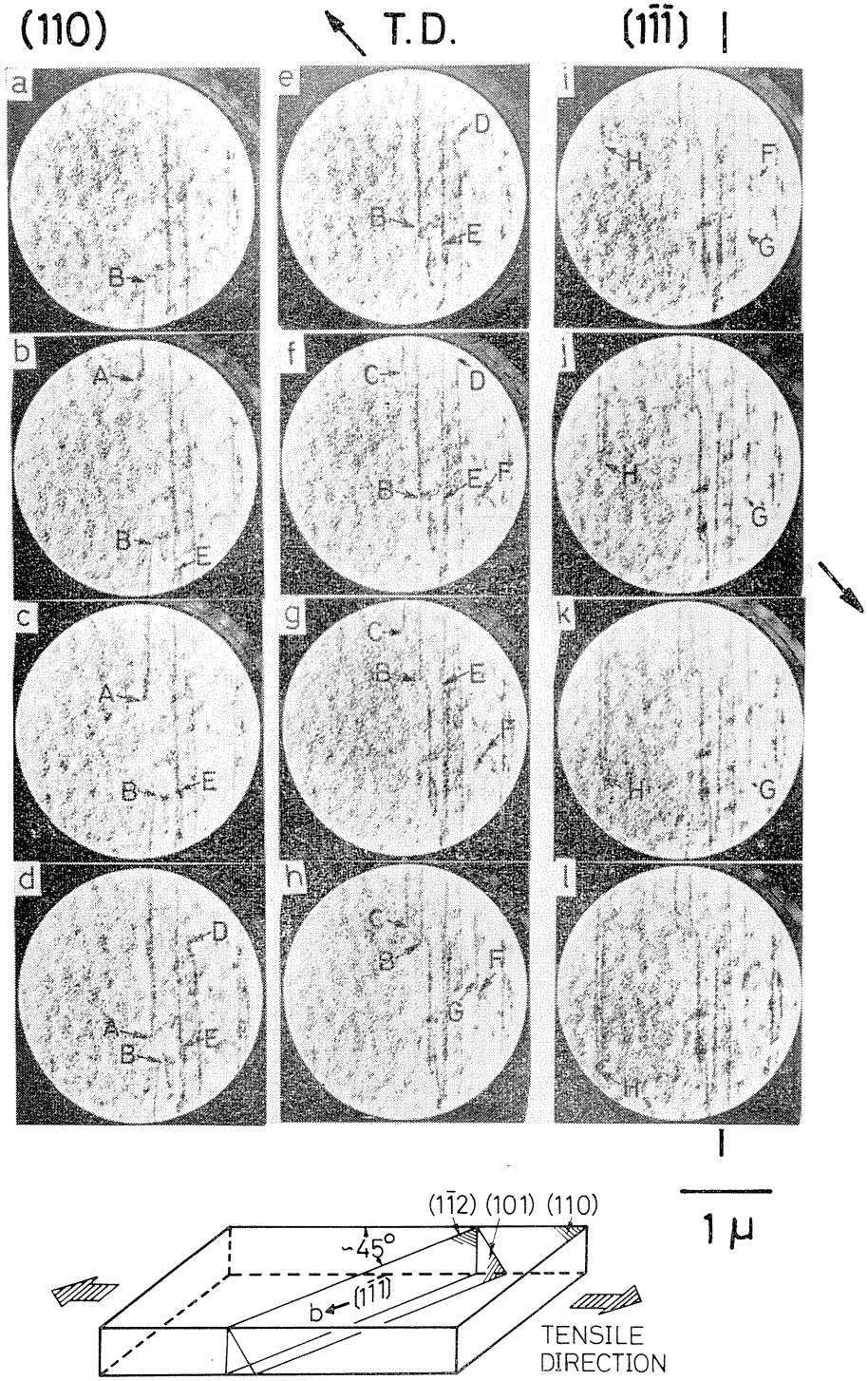

Fig. 23. Example of a sequence of dislocation motion in Fe-3%Si at room temperature.

Fig. 23 reproduces a typical example showing a sequence of the motions of dislocation loops in Fe-3%Si at room temperature[4]. These photographs are taken from the images on a TV screen which are reproduced from VTR at the normal speed (30 frames/sec.) and the intervals between the successive photographs are about 1 sec. Dislocations denoted by A, C, G, and H ran from top to bottom, while dislocations B, D, E, and F ran from bottom to top, indicating that these two groups of dislocations have the same Burgers vector but of opposite signs. Only dislocation F glided on (101) plane, while the remainder on the predicted $(1\bar{1}2)$ primary slip plane.

Velocities of moving dislocations were determined directly from a frame-by-frame analysis of dislocation motion in relation to the stress-strain curve and expressed as a function of the applied stress. With this method the mobilities of edge and screw dislocations in Fe-3%Si[4], Fe[34], and Mo[35] at low and room temperatures have been determined directly. Figs. 24, 25, and 26 show the results on the mobilities of individual dislocations in Fe, Fe-3%Si and Mo, respectively. For all the cases investigated edge dislocations moved much faster than screw dislocations. The scatter of data is fairly large. However, if an empirical relation $v=(\tau/\tau_0)^m$ is used for the velocity-stress relation, the values for the parameters m and τ_0 are obtained for edge and screw dislocations in Fe, Fe-3%Si and Mo at the indicated temperatures and summarized in Table 2.

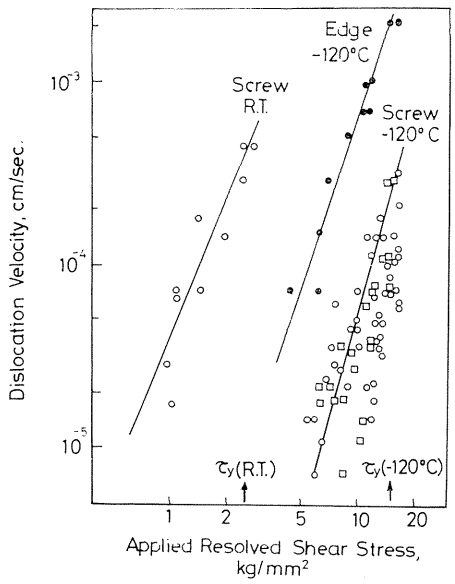

Fig. 24. Mobility of dislocations in Fe.

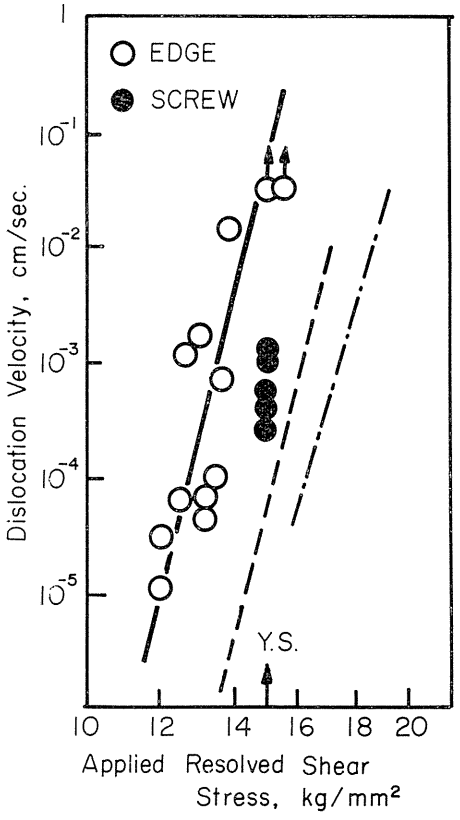

Fig. 25. Mobility of dislocations in Fe-3%Si.

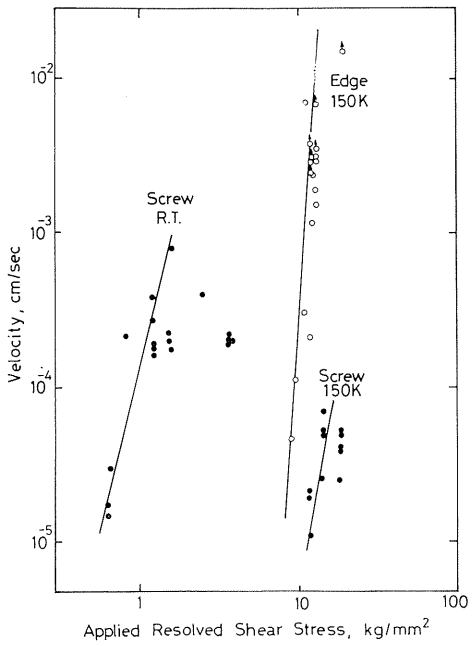

Fig. 26. Mobility of dislocations in Mo.

Table 2. Dislocation mobility parameters m and τ_0 for edge and screw dislocations in Fe, Fe-3%Si and Mo at various temperatures.

	Fe			Fe-3%Si	Mo		
	Room Temp.	−120℃		Room Temp.	Room Temp.	−120℃	
	Screw	Edge	Screw	Edge	Screw	Edge	Screw
m	2.57	3.07	3.82	35±5	5.0−12	13	6.6−11
τ_0, kg/mm²	50	110	130	16±0.5	1.7−6.0	21	34−65

3. 2. 3. *Comparison of the present data with the data obtained with etch-pitting method*

Since Johnston and Gilman[1] succeeded in measuring the velocity of dislocations in LiF crystal as a function of stress by means of a selective dislocation etching method, measurements of dislocation mobility have been made on a variety of crystals with this method.[2, 36~39] In this Johnston-Gilman method, either the displacement of individual dislocations or the propagation of micro-slip bands is measured by comparing dislocation etch-pit configurations before and after the application of a stress pulse with known duration and amplitude, and the velocity of a dislocation v is estimated from the relation

$$v(\tau) = L/\Delta t \tag{3}$$

where L is the distance moved by the dislocation during a stress pulse with stress

amplitude τ and duration Δt. Thus, the dislocation velocity is calculated by assuming that dislocation moves steadily during stress pulse. Actually, however, a dislocation repeats motion and stop and does not move steadily. In this sense the velocity of dislocation obtained with an etch-pitting method is the average velocity of dislocation which repeats motion and stop. On the other hand, the present *in-situ* deformation experiment provides the velocity of dislocations which are actually moving under the action of known stress. In this sense it gives the free-flight velocity of dislocations.

3. 3. Multiplication of Dislocations in Fe Deformed at Low Temperatures

3. 3. 1. Introduction

An understanding of plasticity of crystals necessitates a detailed knowldege of dislocation multiplication in addition to the mobility of individual dislocations, since the density of mobile dislocations is one of the most important factors that govern the plasticity of crystals (cf. Eqns. (1) and (2)).

The density of moving dislocations can be estimated directly as a function of stress or strain, by counting the number of the images of moving dislocations on a monitor TV in the present *in-situ* deformation experiment.

Various types of dislocation multiplication have been observed to operate by *in-situ* deformation experiments[40]. In this section some typical examples of dislocation sources observed in Fe at low temperatures are described. In Fe-3%Si and Mo, essentially similar mechanisms of dislocation multiplication have been observed.

3. 3. 2. Density of moving dislocations

Density of moving dislocations in the stressed crystal can be estimated by counting the images of moving dislocations on TV screen. Fig. 27 shows the density of the moving dislocations in Fe at room temperature and at -120℃. In this figure the applied stress is normalized. Both at room temperature and at -120℃, dislocations began to move well below the yield stress τ_y, although the density was relatively low. The density began to increase rapidly at the stress level of 3/4 τ_y. The density of moving dislocations at the yield point amounted to as large as 5×10^9 lines/cm^2 at room temperature and at -120℃. It should be pointed out, however, that this value of the density of moving dislocations is overestimated due to the preference of recording regions of active dislocation motion and neglecting inactive regions in between.

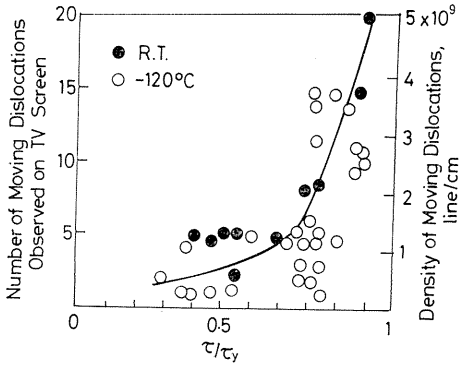

Fig. 27. Density of moving dislocations as a function of the applied stress in Fe.

3. 3. 3. Multiplication of dislocations at super jogs on screw dislocations

Multiplications of dislocations were observed to take place most frequently at super jogs on screw dislocations. Fig. 28 shows such an example. A screw disloca-

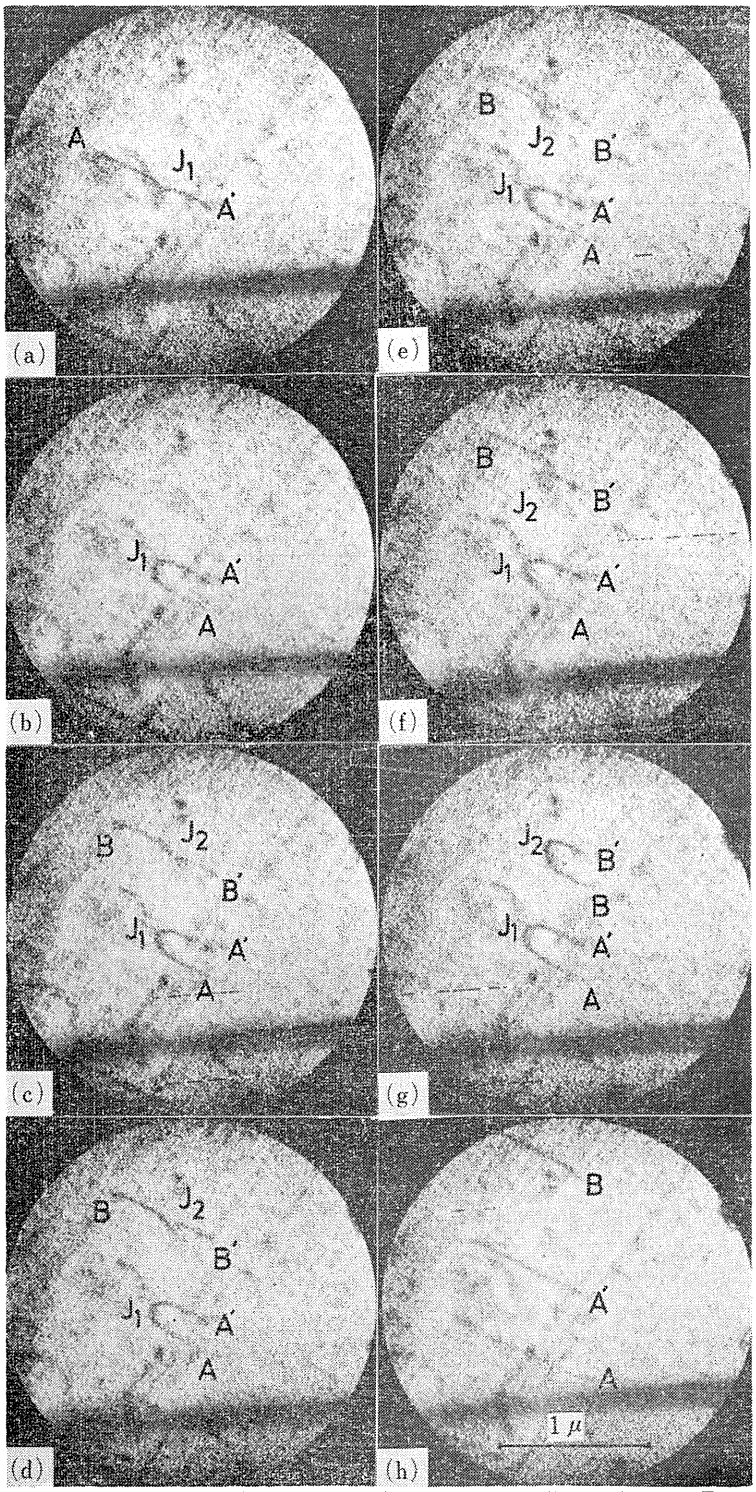

Fig. 28. Dislocation multiplication at super jogs on screw dislocations in Fe at -120℃.

tion AA′ had a jog J_1. The jog J_1 retarded the motion of screw segments AJ_1 and J_1A', and the segment AJ_1 bowed out. Since the mobility of edge component E_1 is much larger than the screw segment AJ_1, E_1 moved faster and reached the foil

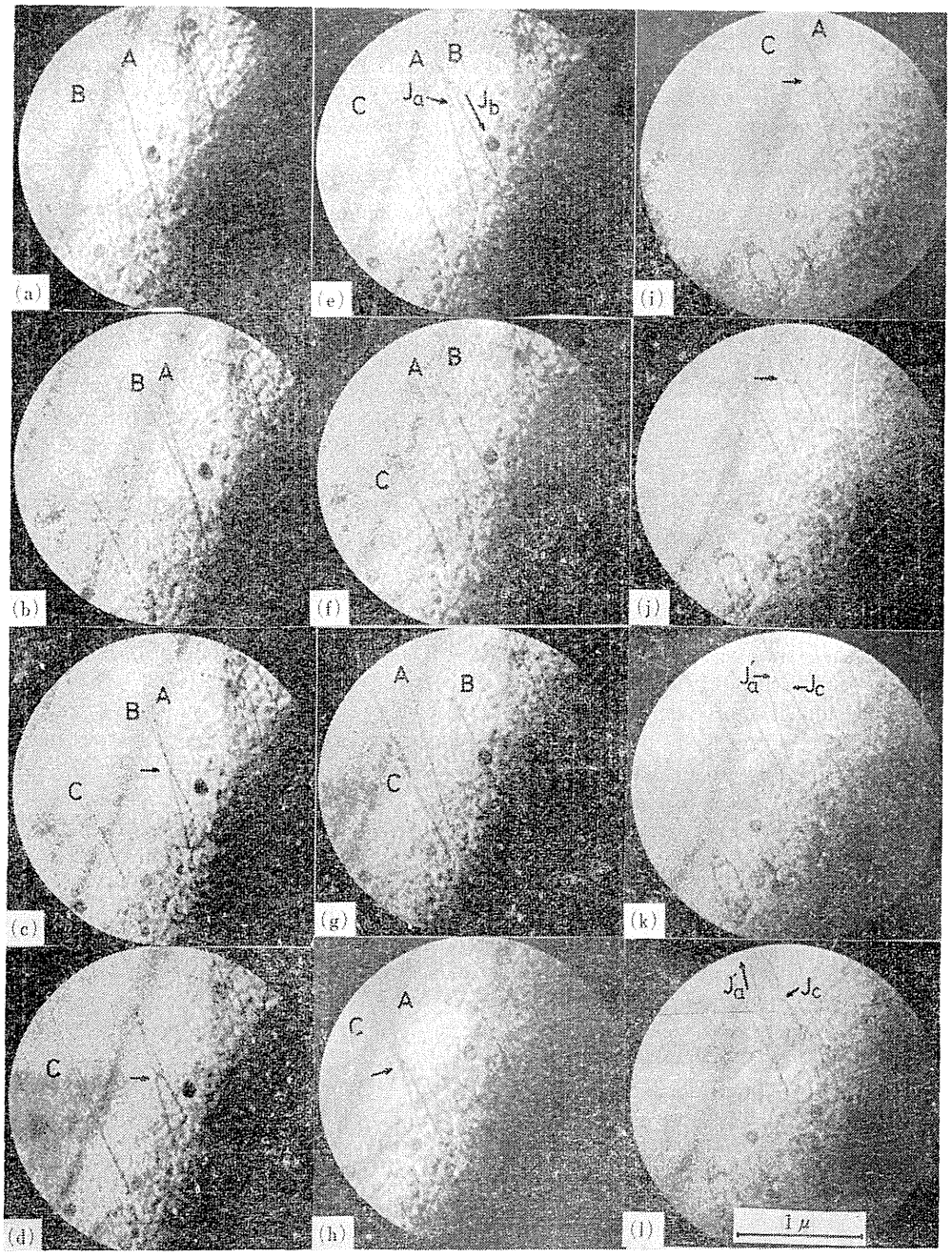

Fig. 29, Crossing of screw dislocations in Fe at -90℃.

surface, leaving a dislocation half-loop AJ_1A behind and emitting a dislocation BB'. In Fig 28(a) a newly emitted dislocation BB' was just in motion during exposure (1/30 sec.) and not seen clearly.

The screw dislocation BB' then acquired a jog J_2 and the motion was retarded again. The same process as mentioned above was repeated between J_2 and BB'. In Fig. 28 (e) the screw segment J_2B has double-image, indicating that it displaced slightly during an exposure of 1/30 sec. Thus, two half-loops AJ_1A' and BJ_2B' were left behind in the foil. Since the jogs J_1 and J_2 were just on edge components of dislocation half-loops in this configuration, they moved together with the edge components and reached the foil surface, each leaving two screw segments (In Fig. 28(h) the segment B' had moved and disappeared .).

Various mechanisms of formation of jogs have been proposed. The present study does not reveal which mechanism is predominant, but an example of the formation of jogs was obtained. Fig. 29 shows a process of the formation of jogs on screw dislocations when they cut each other. Screw dislocations A and B belonged to the different slip systems which operated simultaneously. Both A and B were initially screw-oriented. When they met each other, an apparent interaction occurred as is shown in Fig. 29 (c)-(d). After they cut each other, jogs J_a and J_b were formed on each of the screw dislocations A and B*. It is not clear whether or not the jogs J_a and J_b are elementary jogs or super jogs. If those jogs are formed simply by cutting of two dislocations A and B, then the jogs formed are elementary jogs. On the other hand, if a cross-slip is involved in the process of crossing of A and B, the jogs J_a and J_b thus formed may be super jogs, as is pointed out by Takeuchi.[41]

In the case shown in Fig. 29, the jogs J_a and J_b moved conservatively along the screw dislocations A and B, respectively and disappeared out of the foil. As a result, both A and B became straight and began to move again. The screw dislocation A then met another dislocation C which had the same character as B and the same process described above was repeated between A and C.

In a bulk crystal such processes of formation of jogs and conservative motion of jogs along screw dislocation lines would be repeated; some of the jogs that move along a screw dislocation would meet other jogs that move along the screw dislocation from the opposite direction. If those jogs which meet each other have opposite signs, an annihilation will occur, while they will coarsen to form a larger jog if they have the same sign. Such a larger jog can act as a dislocation source.

3. 3. 4. Frank-Read Source

Dislocation multiplications occurred at dislocation nodes in a way similar to Frank-Read source. Fig. 30 shows a sequence of the operation of such a single-ended source. Branch dislocations A and B rotated around a dislocation node N, emitting a dislocation per each rotation. A dislocation source of the same type is also observed at N'.

The rate of multiplication, *i. e.*, rotation of branch dislocations A and B was governed by their motion when they were in screw orientation, because the velocity of screw component is much lower than that of edge component.

In contrast to the dislocation sources at super jogs (Sec. 3. 3. 3.), both of the

---

* In Fig. 29 (e) jog J_a had moved along screw dislocation A and disappeared out of the foil (see also Fig. 29 (k)).

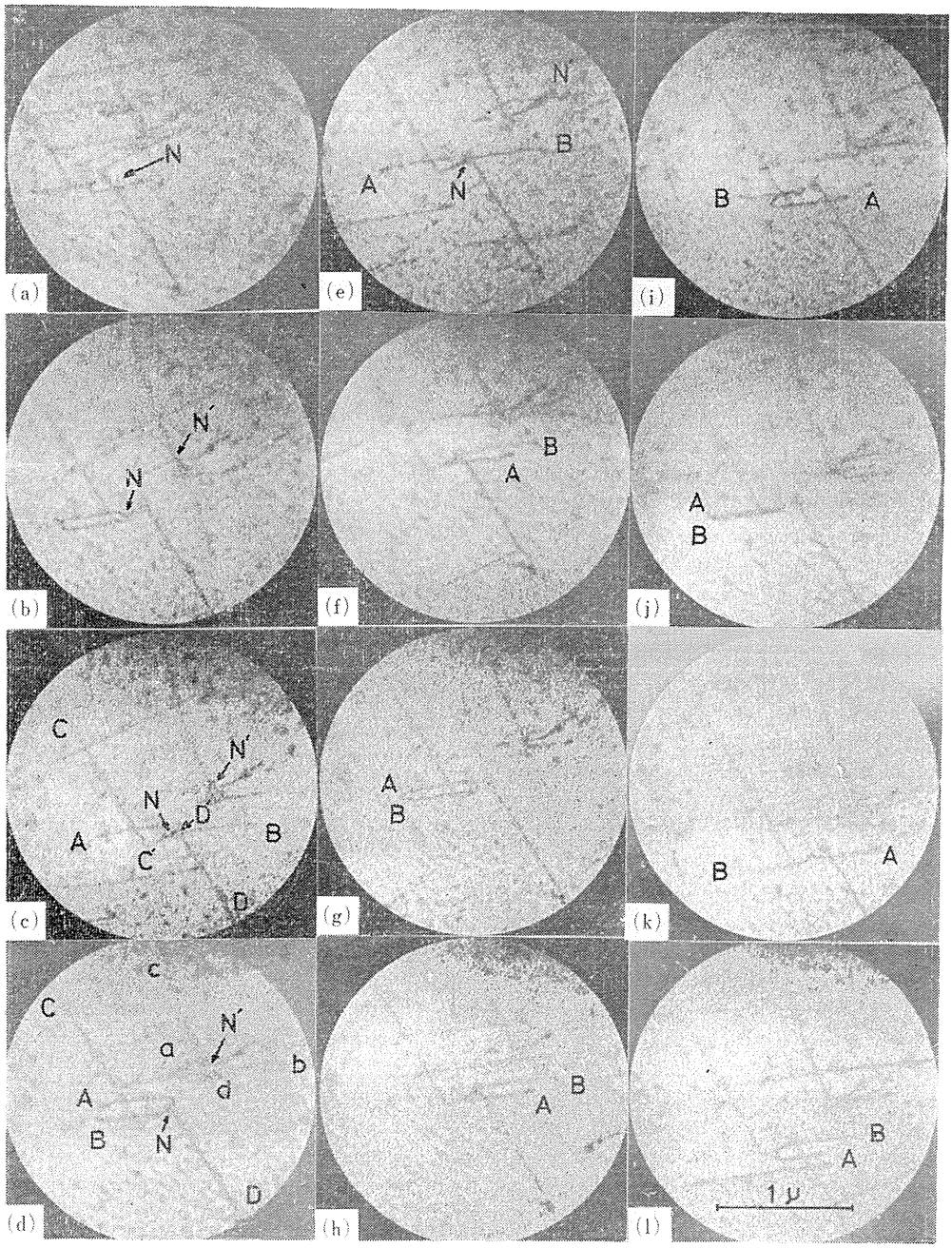

Fig. 30. Frank-Read source in Fe at -150℃.

two branch dislocations A and B rotated. Moreover, the roation was repeated in many times, while in the case of dislocation multiplication at jogs the rotation was limited to only one time. This can be accounted for by taking into consideration

the difference in stability between jogs and dislocation nodes. Jogs can glide conservatively along screw dislocation lines, while nodes are energetically stable and cannot move.

Similar dislocation multiplications have been frequently observed at grown-in sub-boundaries.

3. 3. 5. Dislocation multiplication at inclusion

Dislocation multiplications by the interaction of screw dislocations with inclusion particles were also frequently observed in Fe. Fig. 31 shows an example of the interaction between a dislocation and an inclusion particle. A screw dislocation S was going to by-pass an inclusion particle P. P induced the cross-glide of S. As a result, the dislocation branches A and B of S glided on the slip planes which were separated by the distance of cross-glide and did not meet each other. This process is different from the typical Orowan's by-pass mechanism. Consequently, A and B rotated independently around the inclusion particle P, emitting a dislocation per each rotation. Thus, an inclusion particle enhances the cross-glide of a screw dislocation and provides a dislocation source.

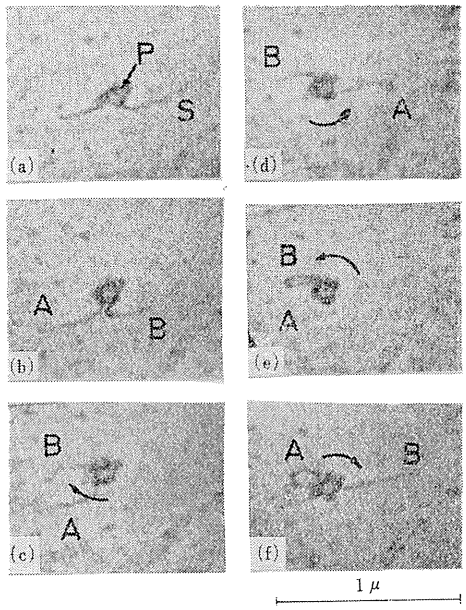

Fig. 31. Interaction of dislocation with inclusion particle in Fe at -120℃.

3. 4. Conclusion

The present *in-situ* deformation experiment shows that in bcc metals at low temperatures edge dislocations move much faster than screw dislocations, leaving screw dislocations behind in the crystal.

The moving screw dislocations had very straight shapes at low temperatures. At high temperatures screw dislocations had less straight shapes and they behaved like flexible strings. This type of motion of screw dislocations at high temperatures was essentially similar to that of edge dislocations at low and high temperatures.

Various types of dislocation source have been observed directly to operate. It is shown that at low temperatures the rate of dislocation multiplication of all of the observed sources is controlled by the motion of dislocations when they are in screw orientation.

Thus, it can be concluded that an increased strength of bcc metals at low temperatures can be attributed to the increased resistance to the motion of a screw dislocation.

4. Anomalous Slips in High-Purity Molybdenum

4. 1. Introduction

It is now well recognized that slips having low Schmid factor take place frequently in high-purity transition bcc metals such as V,[42] Nb,[43~45] Ta,[46] Mo[47~49] and W[49] when they are deformed at low temperatures. The explanations of these low-stressed (anomalous) slips have been made in terms of the core-structure of a screw dislocation,[50] a surface effect model[51, 52] and mechanisms involving double slips.[53, 54] However, there is a controversy on the mechanism responsible for the operation of these anomalous slips. *In-situ* deformation experiments on high-purity Mo single crystals show definitely that in Mo two different types of anomalous slip are activated by the different mechanisms, *i. e.*, a surface-effect mechanism and a co-planar double slip mechanism.

4. 2. Experimental

Mid-oriented single crystal foil specimens of high-purity Mo (annealed in UHV), Fig. 32, were prepared in such a way that the foil surface coincides with the side-face for the primary Burgers vector a/2 [1$\bar{1}$1]. Thus, the primary Burgers vector

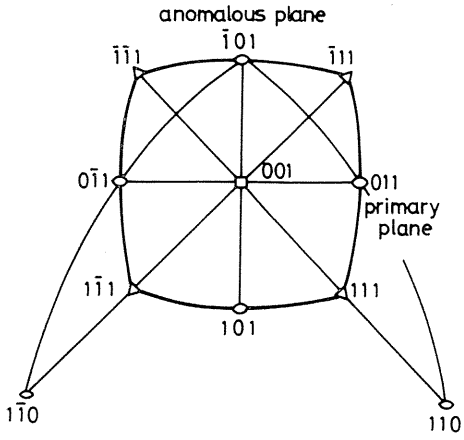

Fig. 32. Orientation of tensile direction.

lies nearly parallel to the foil surface, Fig. 33.

Trace analysis was carried out on the slip lines appearing on the surface of foil specimens stretched in HVEM as well as on the slip trails of those individual dislocations which moved under the action of the applied stress during *in-situ* deformation experiments and the active slip systems were determined. The behaviour of individual dislocations was observed in detail and the features characteristic of the dislocation behaviour in the respective slip systems were analysed. This allowed the identification of the mechanisms which control the operation of the respective slips.

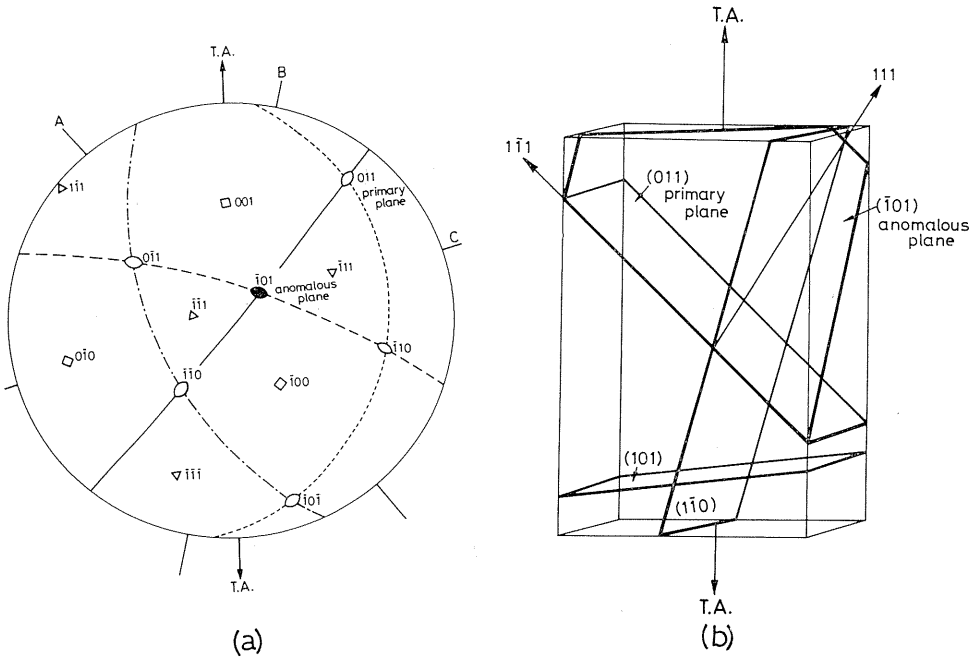

Fig. 33. (a) Stereographic projection of the foil surface.
(b) Geometry of slip systems in foil specimen.

4. 3. Results

4. 3. 1. Slip system determination

Fig. 34 (a) shows an optical micrograph of the surface of a specimen stretched under observation in HVEM. Three sets of slip lines denoted by A, B, and C can be observed. The corresponding transmission electron micrograph is presented in Fig. 34 (b). A prominent feature of dislocation structure shown in Fig. 34 (b) is that apparently straight and long dislocations are predominant. The Burgers vector determination by a contrast experiment during an *in-situ* experiment showed that they are all in screw orientation; they were left behind in the wake of edge components which had moved away due to a larger mobility.

Trace analysis was carried out on Fig. 34 and also on the slip trails of those individual dislocations which moved during an *in-situ* deformation experiment under the action of the applied stress. In addition, the surface of foil specimen stretched in HVEM was examined by SEM as well as interferography. These results were compared with the results of the aforementioned trace analysis and the active slip systems were determined unambiguously.

Table 3 lists the observed slip systems in Mo in the present *in-situ* experiment, together with the selected parameters. The features of dislocation behaviour characteristic of the respective slip systems are also remarked. Many slip systems operated from the onset of deformation. Except the primary $[1\bar{1}1]\,(011)$ slip system the observed slip systems had low Schmid factors. Two types of anomalous slip are distinguished from the features of dislocation behaviour characteristic of the slip bands. These will be described in the following.

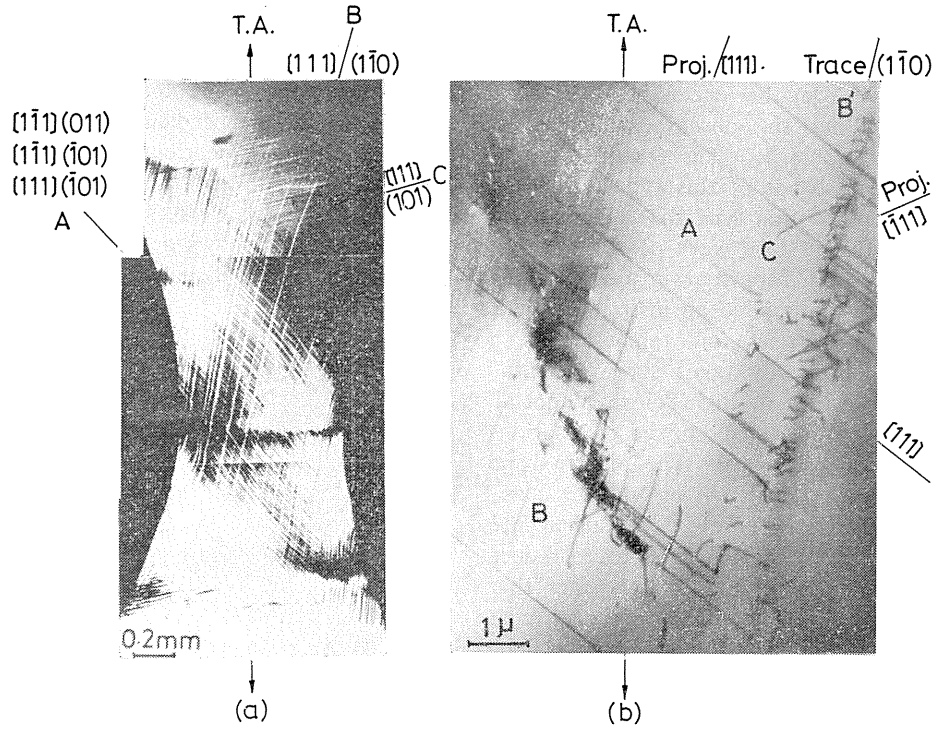

Fig. 34. (a) Optical micrograph of foil specimen of Mo stretched in HVEM.
(b) Transmission electron micrograph of Mo foil specimen stretched in HVEM.

Table 3. Slip systems observed in Mo.

b	Slip plane	β	α	Schmid factor	Features of dislocation behaviour
[1$\bar{1}$1]	(011)*	88°	80°	0.49	Dislocation loops elongated along ***b***
	($\bar{1}$01)*†	88°	20°	0.15	Motion of dislocation networks
	(110)	88°	43°	0.35	
[111]	(0$\bar{1}$1)	73°	55°	0.41	
	($\bar{1}$01)*†	73°	20°	0.20	Motion of dislocation networks
	($\bar{1}$10)*	73°	71°	0.19	Isolated straight screws and trains of curved mixed dislocations
[$\bar{1}$11]	(0$\bar{1}$1)	53°	55°	0.15	
	(110)	53°	43°	0.17	
	(101)*	53°	82°	0.31	Isolated straight screws
[$\bar{1}\bar{1}$1]	(011)	20°	80°	0.04	
	($\bar{1}$10)	20°	71°	0.01	
	(101)	20°	82°	0.05	

β =angle between Burgers vector and surface normal
α =angle between surface normal and normal to the slip plane
* Observed slip systems
† ($\bar{1}$01) anomalous slips

4. 3. 2. Anomalous slip activated by S. E. mechanism

Anomalous slips of this type are [111](1̄10) and [1̄11](101) and they are observed from the onset of deformation. The most prominent feature of these slips is that the observed slip planes are most nearly perpendicular to the foil surface (Table 3). The feature of behaviour of individual dislocations characteristic of the slip bands of this type is the usual motion of dislocations. In addition, in the slip bands of this type the trains of mixed dislocations which were steeply inclined to the foil surface were observed very frequently. Fig. 35 shows a typical example of dislocation behaviour in a slip band of this type. Many dislocations of mixed orientation are piled up in the slip band. In bcc metals at low temperatures, a dislocation usually takes screw orientation because of its high Peierls potential. The fact that many mixed dislocations were observed in this type of slip band indicates that they converted their character from the screw orientation into the mixed orientation in order to reduce their lengths. In addition, the fact that the slip planes of this type are most nearly perpendicular to the foil surface suggests that the free surface has a profound effect on the operation of these anomalous slips.

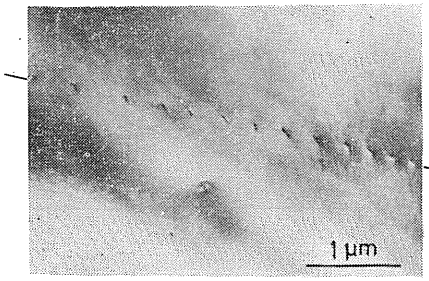

Eig. 35. An example of dislocation behaviour in the slip band activated by S. E. mechanism.

Vesely[47] found that slip lines appearing on the surface of a Mo single crystal depend sensitively on the local orientation of the crystal surface. More recently Matsui and Kimura[51] have proposed a specific mechanism for the operation of the surface-induced slip in bcc metals. In their mechanism (S. E. mechanism) part of a screw dislocation emerging at the surface is deflected by the image force into the plane most nearly perpendicular to the local crystal surface, thereby having non-screw character. Under the action of the applied stress, the non-screw part of the dislocation near the surface glides towards the interior of crystal; its glide plane is that plane into which the near-surface part of the originally screw-oriented dislocation is deflected by the image force. Thus, the slip system which is perpendicular to the surface is activated. The observations of the present *in-situ* deformation experiment show definitely that the S. E. mechanism operates to activate the anomalous slips of this type in Mo.

4. 3. 3. Anomalous slip activated by C. D. S. mechanism[72, 73]

Anomalous slips of this type, namely [1$\bar{1}$1](1̄01)/[111](1̄01) are the so-called (1̄01) anomalous slips. These slips cannot be explained in terms of the S. E. mechanism, since (1̄01) is the plane most nearly parallel to the foil surface (Table 3). Fig. 36 shows a typical example of the dislocation behaviour in this type of anomalous slip. In Fig. 36 (a) two sets of straight and long dislocations of screw character A and B are observed; they have the Burgers vector a/2 [1$\bar{1}$1] and a/2 [111], respectively. In Fig. 36 (b) two dislocation networks N and N′ are observed to have been formed, the schematic sketch being shown in Fig. 37 (a). Of these two

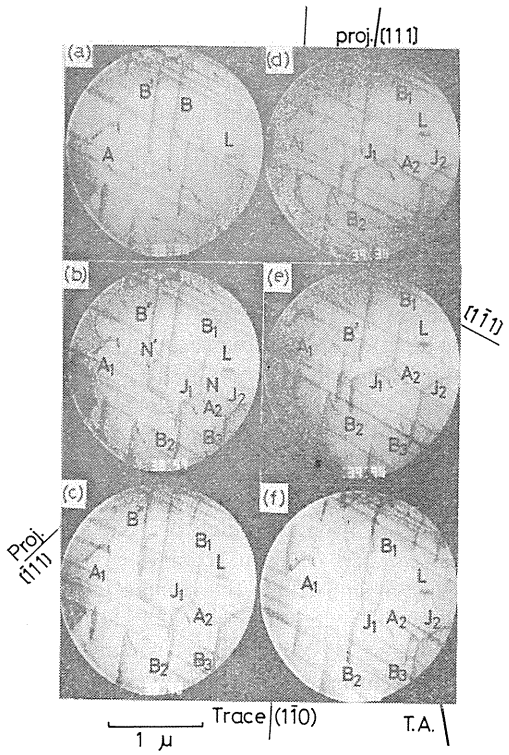

Fig. 36. Example of dislocation behaviour in ($\bar{1}$01) anomalous slip.

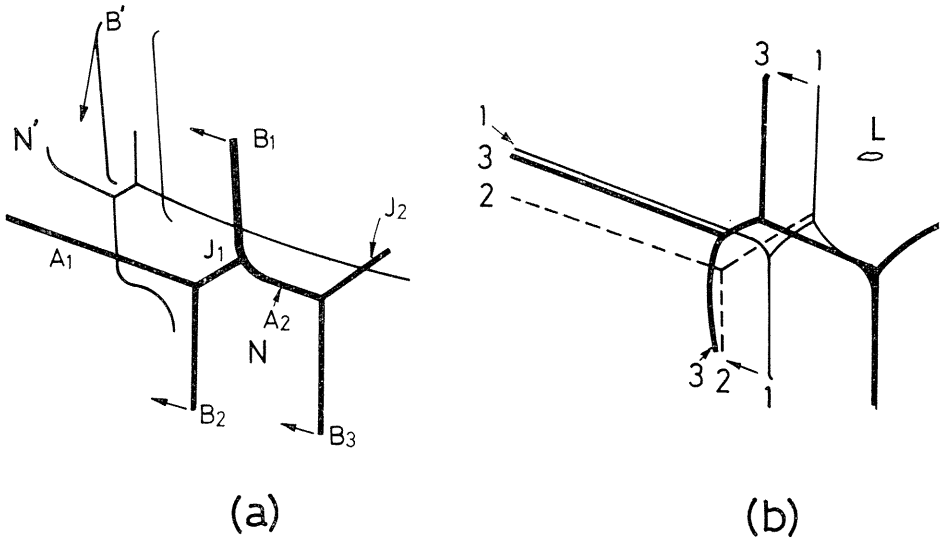

Fig. 37. (a) Schematic sketch of Fig. 36 (b) to show more clearly the configurations of N and N'.
(b) Superimposition of dislocation segments of N in Fig. 36.

networks N and N′, the latter N′ decomposed subsequently and moved away out of sight. The former network N, the behaviour of which will be described in detail in the following, is composed of seven dislocation segments, as depicted in Fig. 37 (a). Thus, the dislocation network N is formed as a result of the reaction

$$a/2[\bar{1}1\bar{1}]+a/2[111]=a[010] \tag{4}$$

A striking feature of the dislocation behaviour shown in Fig. 36 is that the dislocation network N moved as a whole (In Fig. 37 (b) the configurations of each of the segments comprising the network are delineated and superimposed to show more clearly the displacement of each segments.). It is to be noted that not only the reactant a/2 <111> dislocations which were originally glissile but also the junction dislocation having the Burgers vector a[010] move simultaneously. This process is possible in the case where all the dislocations comprising the network move on one common slip plane on which lie the three types of Burgers vectors concerned, *i. e.*, a/2 [1$\bar{1}$1], a/2 [111] and a [010]. From Fig. 32 it can be seen that this common plane coincides with the so-called anomalous ($\bar{1}$01) plane.

The isolated a/2 [111] dislocation B′ which did not form a dislocation network moved on the ($\bar{1}$10) plane, as can be seen from the trace of motion shown in Fig. 36 (c) to (e). Thus, it can be said that the formation of a dislocation network induces the anomalous ($\bar{1}$01) slip. That is, the a/2 [1$\bar{1}$1] dislocation which moves on (011) plane reacts with the a/2 [111] dislocation which moves on the ($\bar{1}$10) plane to form the a[010] junction dislocation. As a result, the reactant a/2[1$\bar{1}$1] and a/2 [111] dislocations can no longer continue to move on their original slip planes. Instead, they cross-slip onto the ($\bar{1}$01) anomalous slip plane, which is the common plane of the reactant and the product dislocations and continue to move on the ($\bar{1}$01) anomalous slip plane, together with the junction dislocation, keeping the shape of dislocation network as a whole.

The aforementioned features of dislocation behaviour in the ($\bar{1}$01) anomalous slip are in good agreement with the co-planar double slip model proposed by Matsui and Kimura[53] for an explanation of the ($\bar{1}$01) anomalous slip in bcc metals.

4. 4. Conclusion

It is experimentally confirmed that two different types of anomalous slip are activated in Mo; the so-called ($\bar{1}$01) anomalous slip is activated by the C. D. S. mechanism, the other by the S. E. mechanism. In the VIa group bcc metals such as Mo and W, both the S. E. and C. D. S. mechanisms operate in the initial stage of hardening, resulting in very complex slip geometries. In the Va group bcc metals such as Nb, Ta and V on the other hand, only the C. D. S. mechanism operates. The difference may be attributed to subtle difference in surface condition.

5. Behaviour of Dislocations during Unloading

5. 1. Introduction

By irradiating with fast neutrons deformed copper single crystals before removing the applied load, Crump III and Young[55] and Mughrabi[56] succeeded in investigating by TEM important features of the dislocation arrangement in the

stress-applied state. The observations of these workers suggest that a considerable rearrangement of dislocations takes place when a stressed crystal is relaxed. This technique, however, cannot allow the comparison of the arrangement of dislocations in the stress-applied state with that of the same dislocations in the stress-removed state; change in configuration of the same dislocations during unloading cannot be followed directly. Therefore, the behaviour of individual dislocations during unloading is masked in this technique by the statistical scatter inherent to the dislocation arrangement in deformed crystals.

The behaviour of dislocations during unloading in Ni[57] and Mo[58] single crystals have been observed by *in-situ* deformation experiment in HVEM. The change in configuration of dislocations is analysed in relation to the stress-strain curve and this allows the estimation of the effective, frictional and internal stresses acting on the individual dislocations.

5. 2. Experimental

Single crystal foil specimens of high-purity Ni and Mo were stretched while under observation in HVEM. At some appropriate points on the stress-strain curve the straining was interrupted and the load was removed, and then again increased until the crystal yielded. The behaviour of individual dislocations during this stress cycle was recorded continuously.

5. 3. Behaviour of Dislocations during Stress Cycle in Ni[57]

5. 3. 1. Virgin crystals

Fig. 38 shows the stress-strain curve of a Ni foil specimen. A typical example of the dislocation behaviour during a stress cycle is reproduced in Fig. 39 (a)-(g), where (a) to (g) correspond to the points (a) to (g) indicated on the stress-strain curve (Fig. 38). Two dislocations A and B of the conjugate slip system which

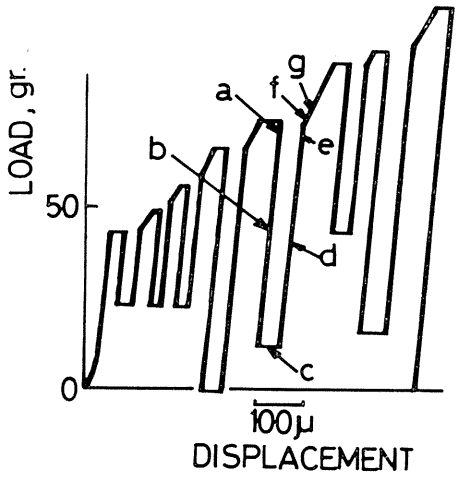

Fig. 38. Stress-strain curve. The curve is shifted intentionally along the strain axis for clarity at the points where unloading and reloading started.

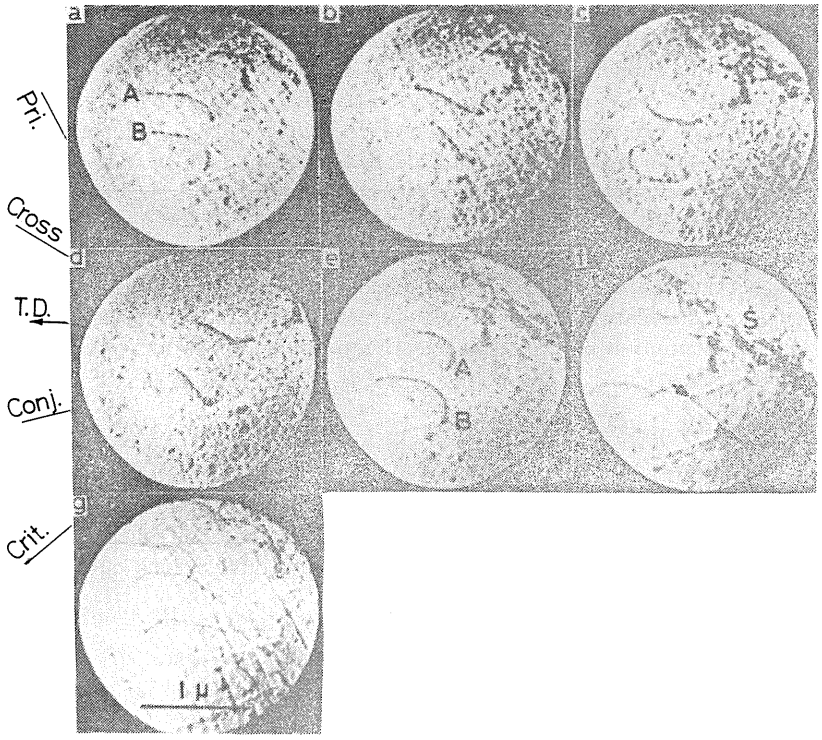

Fig. 39. Behaviour of dislocations during unloading-reloading stress cycle in annealed Ni.

bowed out to the right in the stress-applied state (a) shrank as the applied stress was reduced. At the stress level about half of the flow stress (hereafter denoted by τ_f) at which unloading started, both A and B became straight in this particular case (b). On further reducing the applied stress, they began to bow out to the left (in the reverse direction), as is shown in (c). On reloading, they became straight at the stress level just half of τ_f (d) and bowed out to the right again (e), as the applied stress exceeded 1/2 τ_f. Immediately after τ_f was reached (f), long-range motions of dislocations A and B started and the slip trails of those dislocations which came out of sight covered the area being observed (g). This indicates that the specimen yielded. At the same time an apparent yield point appeared on the stress-strain curve.

5. 3. 2. Prestrained crystals

A similar stress cycling experiment was carried out on Ni foil specimens which were prepared from a crystal elongated to 13% in the bulk state in order to examine the effect of pre-existing dislocations. An example is shown in Fig. 40. In this case four dislocations A, B, C and D are observed within the cell which was formed during prestraining. All of these dislocations bowed out to the right in the stress-applied state (a). However, the curvatures of these dislocations differed from dislocation to dislocation; the dislocations A and B are more curved than the dislocations C and D. This indicates that the effective stress acting on A and B is

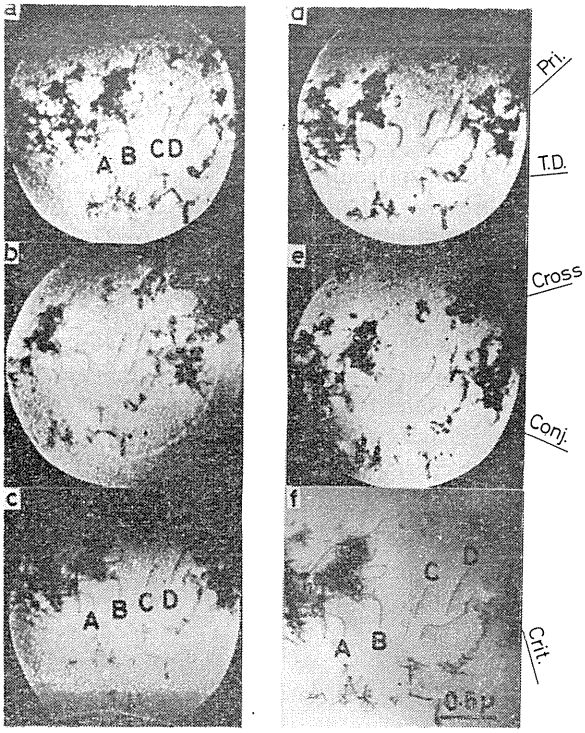

Fig. 40. Behaviour of dislocations during unloading-reloading stress cycle in prestrained Ni.

larger than that acting on C and D.

As the applied stress was decreased, C and D shrank and straightened and finally bowed out in the reverse direction. This behaviour is essentially similar to the behaviour of dislocations described already. In contrast, dislocations A and B did not become straight in the stress-removed state, although they shrank a little. On reloading, C and D shrank, straightened and finally bowed out to the right again. Dislocations A and B bowed out further to the right.

5. 3. 3. Effective stress, internal stress and frictional stress in Ni

General considerations

According to the line-tension approximation of a dislocation, the effective stress acting on a dislocation can be expressed by

$$\tau^* = Gb/R \tag{5}$$

where G is shear modulus, b is the strength of Burgers vector and R is the radius of curvature of a curved dislocation under consideration. Thus, from the curvature of the dislocation being observed in EM the effective stress acting on the dislocation can be estimated from Eqn. (5).

The effective stress can be considered as the sum of the applied stress and internal stress

$$\tau^* = \tau_a + \tau_i \tag{6}$$

Therefore, the internal stress can be determined from the effective stress acting on the dislocation in the stress-removed state ($\tau_a=0$). Alternatively the ratio of the internal stress can be estimated from the stress level on the stress-strain curve where the effective stress is zero, that is, the dislocation under consideration is straight ($R=\infty$). In such a case, $\tau^*=0$, so that $\tau_i=-\tau_a$.

In the present study the displacements of individual dislocations during stress cycles were measured directly. If one dislocation sweeps an incremental area ΔS, then it produces an incremental plastic strain $\Delta\varepsilon_p$

$$\Delta\varepsilon_p=b\cdot\Delta S/V \tag{7}$$

where V is the volume of the crystal. Thus, $\sigma-\Delta\varepsilon_p$ curve can be obtained for each of the individual dislocations during a stress cycle. In this connection, the technique can be regarded as a kind of micro-strain experiment. The "extensometer" of this technique has a highest sensitivity. The area of the loop of $\sigma-\Delta\varepsilon_p$ curve during a stress cycle determines the energy loss per cycle

$$W=\oint\sigma_f\cdot d\varepsilon_p \tag{8}$$

where σ_f is the frictional stress acting on the dislocations. Thus, the frictional stress acting on the dislocations can be estimated by analysing the $\sigma-\Delta\varepsilon_p$ curves for the dislocations concerned.

Virgin crystal

As was described already, the dislocations A and B in Fig. 39 became straight when applied stress was reduced to one-half of the flow stress τ_f. In such a case, $\tau_a=1/2\tau_f$ and $\tau^*=1/2\tau_f+\tau_i=0$, so that $\tau_i=-1/2\tau_f$. That is, the internal stress acting on the dislocations A and B in the stress-applied state is about half of the flow stress in this particular case. From Eqn. (6) it is clear that the effective stress is also just half of the flow stress τ_f.

The curves A and B in Fig. 41 (a) show the $\sigma-\Delta\varepsilon_p$ curves of the dislocations A and B shown in Fig. 39. Within the accuracy of the experiment the energy loss per cycle is zero, that is, $W=0$, indicating that the frictional stress acting on the dislocations in annealed Ni is very small.

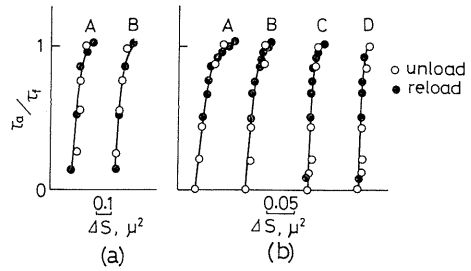

Fig. 41. (a) σ-$\Delta\varepsilon_p$ curves for dislocations A and B of Fig. 39.
(b) σ-$\Delta\varepsilon_p$ curves for dislocations A, B, C and D of Fig. 40.

Prestrained crystals

In the prestrained crystals, the effective stress acting on dislocations A, B, C and D of Fig. 40 was calculated and plotted for the stress-applied states, for partially relaxed states and for the fully relaxed state in Fig. 42. From Eqn. (6) the effective stress acting on the dislocations in the stress-removed state ($\tau_a=0$) τ_r^* corresponds to the internal stress, that is, $\tau_i=\tau_r^*$; the difference in effective stress between the stress-applied state (τ_s^*) and the stress-removed state (τ_r^*) must be equal to the flow stress, that is, $\tau_f=\tau_s^*-\tau_r^*$.

From Fig. 42 it is clear that the local internal stress changes from dislocation

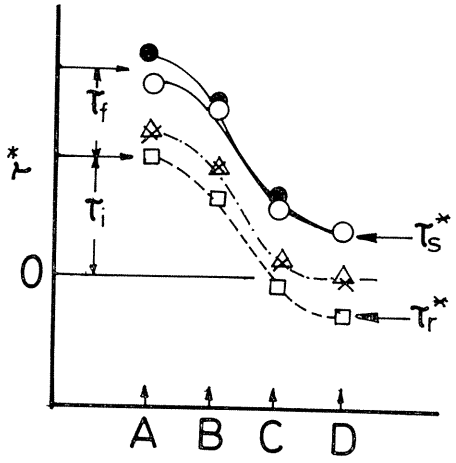

Fig. 42. Variation of effective stress acting on dislocations A, B, C and D of Fig. 40.

to dislocation. The internal stress acting on the dislocations A and B is nearly equal to the flow stress but the internal stress acting on D is about half of the flow stress in magnitude but of opposite sign. The internal stress acting on C is nearly zero. Thus, in this particular case the internal stress oscillates between $-1/2\tau_a$ and τ_a. It is clear that the dislocation tangles T_1 and T_2 exert long-range repulsive forces on these dislocations.

$\sigma-\Delta\varepsilon_p$ curves for the dislocations A, B, C and D in Fig. 40 are reproduced in Fig. 41 (b). Here again the area W of the loops of $\sigma-\Delta\varepsilon_p$ curves is equal to zero, indicating that the frictional stress acting on the dislocations in the prestrained Ni is negligibly small.

5. 4. *Dislocation Behaviour during Stress Cycle in Mo*[58]

5. 4. 1. *Behaviour of dislocation loop*

Fig. 43 shows an example of the behaviour of a dislocation loop at room temperature during unloading in Mo. The mobility of edge dislocations in Mo at room

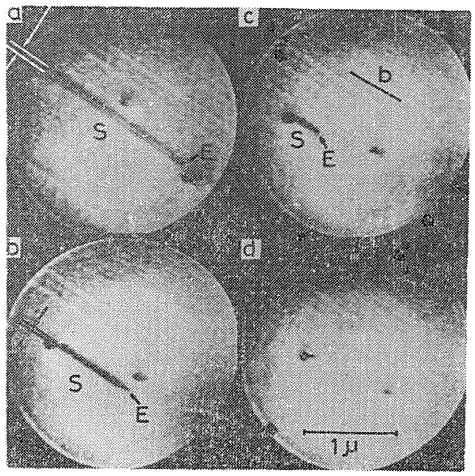

Fig. 43. Behaviour of dislocation loop in Mo during unloading.

temperature is much higher than that of screws (cf. Fig. 26). Thus, in the stress-applied state the edge components of a dislocation loop moved in preference to the screw components, resulting in the dislocation loop being elongated along the direction of Burgers vector, as is shown in Fig. 43(a). As the applied stress was

decreased, the dislocation loop shrank; the edge component moved backwards and the separation of a pair of screw components reduced, (b)-(d). Thus, not only the edge components but also the screw components of a dislocation loop in Mo move reversely during unloading at room temperature. The behaviour of a J-shaped dislocation half-loop of which the edge component emerged at the foil surface was also observed, as in Fig. 44. The edge component of a J-shaped half-loop moved forwards along the direction of the Burgers vector in the stress-applied state, (a)-(c). During unloading it moved backwards, (d)-(f). When the applied stress

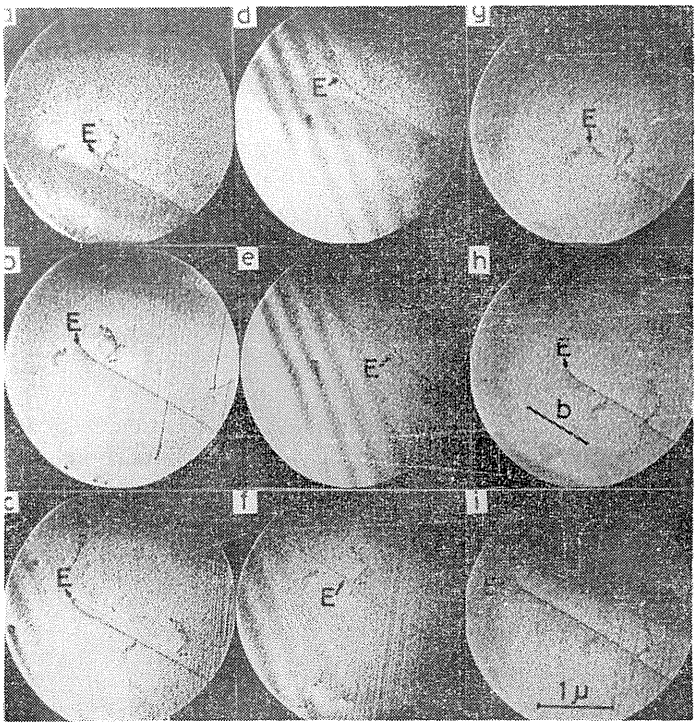

Fig. 44. Behaviour of dislocation half-loop during unloading-reloading stress cycle in Mo.

was increased again, it moved forwards again, (g)-(i). Thus, the edge component behaved quite reversibly in respect to the change of the applied stress. This behaviour of the J-shaped half-loop is essentially similar to that of the U-shaped dislocation loop mentioned above, except that the motion of edge component of J-shaped half-loop was very jerky; in contrast, the motion of the edge component of the U-shaped loop was relatively smooth.

5. 4. 2. Behaviour of screw dislocation

Since the mobility of edge dislocations in Mo at room temperature is higher than that of screws, the edge components of dislocation loops move in preference to the screws, leaving the straight screws behind. The screw dislocations which move under the action of the applied stress have highly straight shapes but they

become wavy in the stress-removed state. Fig. 45 shows an example of this behaviour of screw dislocations during an unloading-reloading stress cycle. The screw dislocations which had straight shapes in the stress-applied state ($\tau_a=\tau_f$), (a) became wavy as the applied stress was reduced ($\tau_a<\tau_f$), (b). When the applied stress τ_a was again increased until the original stress level τ_f was reached ($\tau_a=\tau_f$), those screw dislocations which were wavy in the stress-removed state became straight again, (c) and began to move actively.

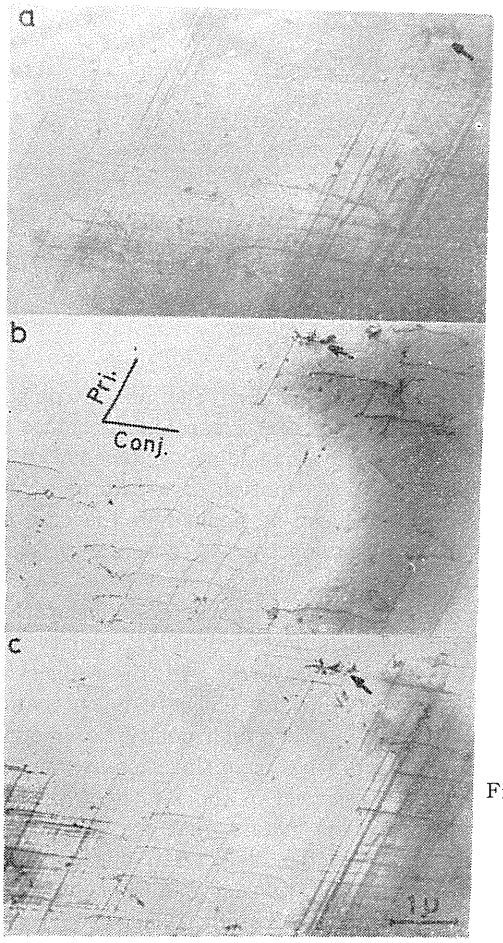

Fig. 45. Variation in configuration of screw dislocations during unloading-reloading stress cycle in Mo.

5. 4. 3. *Discussion*

The present *in-situ* observation shows definitely that a substantial rearrangement of dislocations takes place in Mo at room temperature during unloading; during unloading not only edge components but also screw components of a dislocation loop moved backwards, resulting in the shrinkage of the dislocation loop. The backward motion of the edge components of a dislocation loop can be explained in terms of the back stress due to the line-tension of the dislocation line. The backward motion of screw components can be explained as follows. Fig. 46 shows schematically a

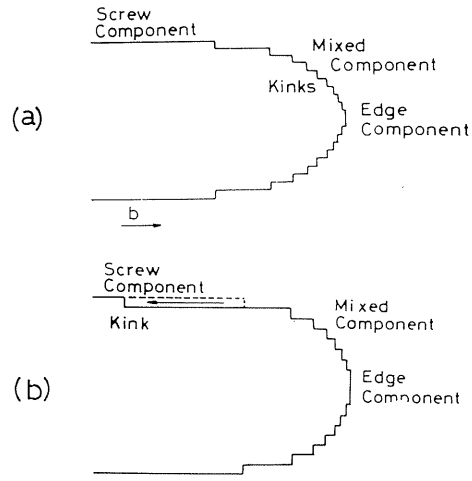

Fig. 46. Schematic illustration of dislocation loop elongated along the direction of Burgers vector.

dislocation loop elongated along the direction of Burgers vector; the mixed component of the dislocation loop consists of high density of geometrical kinks. Since a kink has an edge character, it can move backwards during unloading, as schematically shown in Fig. 46 (b). As a result, an apparent backward motion of a pair of screw components takes place. Essentially similar discussion can be applied to the case of a J-shaped dislocation half-loop, since a J-shaped half-loop can be considered as a part of a U-shaped dislocation loop.

In this study the behaviour of dislocations of various characters (dislocation loop, dislocation half-loop and screw dislocation) was observed in high-purity Mo during an unloading-reloading stress cycle at room temperature. All these dislocations change their configurations substantially during unloading. There is no reason to deny that a similar rearrangement takes place in other high-purity bcc metals than Mo. This gives rise to a great problem in interpreting the dislocation structures of deformed bcc metals. It has been implicitly assumed in the interpretation of TEM observations of the dislocation structure of bcc metals that no substantial rearrangement takes place during unloading and that the dislocation arrangement observed in foil specimens prepared from deformed and relaxed metals represents the arrangement in the stress-applied state. The present study indicates clearly that it is not the case. Especially the difference in the shape of screw dislocations between the stress-applied state and the stress-removed state is essential, since the plasticity of bcc matals is controlled by screw dislocations (cf. Chapter 3). Thus, if one wants to observe the dislocation arrangement in the stress-applied state, it is necessary to freeze-in the dislocation structure by irradiating with neutrons before removing the load, as was done for Cu.[55,56] A long-range backward motion of the J-shaped dislocation half-loop is closely connected with the accuracy of measurement of the velocity of dislocations by a conventional etch-pitting method. The velocity of dislocation was measured by comparing the dislocation arrangements before and after applying a stress pulse (hence necessarily in the stress-removed state). In

the case where a long-range backward motion of a dislocation takes place during unloading, the velocity obtained in this method is underestimated.

6. Behaviour of Dislocations in Irradiated Metals

6. 1. Introduction

The plasticity of irradiated metals is of theoretical as well as practical interest and many attempts have been made to correlate the mechanical properties of irradiated metals with the deformation microstructure. The most striking feature which characterizes the microstructure of irradiated metals is the so-called dislocation channels where the defect clusters introduced by irradiation have been eliminated completely[59]. Thus, an understanding of the plasticity of irradiated metals necessitates a detailed knowledge on the mechanisms of formation, propagation and hardening of the dislocation channels.

Makin[60] showed that the electron beam of HVEM can produce point defect clusters in the crystal being examined in case the energy of incident electron exceeds a threshold value. Since then, many *in-situ* irradiation studies have been made on a variety of metals by using HVEM.[61, 62] By combining the *in-situ* irradiation experiment with the *in-situ* deformation experiment, it is possible to observe directly the interaction between the moving dislocations and defect clusters.[63, 64]

From an industrial viewpoint, neutron-irradiation is more important than electron-irradiation. To study the nature of neutron-irradiation hardening of metals, an *in-situ* deformation experiment was carried out on neutron-irradiated Ni single crystals and the formation of dislocation channels was observed directly.[65]

6. 2. Experimental

The materials used in this study are single crystals grown from high-purity Ni (99.99%) purchased from Johnson Matthey and Co. Ltd.

6. 2. 1. Electron-irradiation

A foil specimen which was mounted to a tensile device was irradiated *in situ* by electrons accelerated at a voltage of 600kV, 800kV and 1000kV in HVEM. In this case, the electron beam was concentrated onto a limited region of the specimen, so that only the intentionally irradiated region was damaged, while no damage occurred in the remainder of the specimen. Then, the specimen was stretched *in situ* while under observation at 400kV (below the threshold value for producing radiation damage in Ni, 440kV[66]). The behaviour of individual dislocations was observed both in the damaged and in the undamaged regions and compared one with other. Thus, a direct comparison of the dislocation behaviour inside and outside the damaged region was made possible.

6. 2. 2. Neutron-irradiation

Foil specimens were sealed in quarz capsules in an atmosphere of helium gas and irradiated by neutrons at a reactor ambient temperature to a fluence of 4.5×10^{18} fast neutrons/cm^2 in KUR of Kyoto University. These specimens were stretched *in situ* while under observation in a JEOL 1 MV microscope of Japan Atomic Energy Research Institute at Tokai-mura (operaing at 400kV).

6. 3. *Results and Discussion*

6. 3. 1. *Electron-irradiated Ni* [64, 67]

Fig. 47 shows the microstructure of a Ni foil which was irradiated with 1000kV electrons to a fluence of 3.8×10^{19}e/cm^2. The point defect clusters of several hundreds Å in diameter were dispersed uniformly in the matrix. The behaviour of dislocations under the action of the applied stress in such a damaged crystal is very much different from that in an undamaged crystal. Fig. 48 shows a typical example of a sequence of the deformation in the damaged and in the undamaged regions of Ni. The region in the lower right corner of the micrographs denoted by D was severely damaged (irradiated with 600kV electrons, 4.6×10^{21} e/cm^2), while the remainder was undamaged. Close investigations of these micrographs and similar others re-

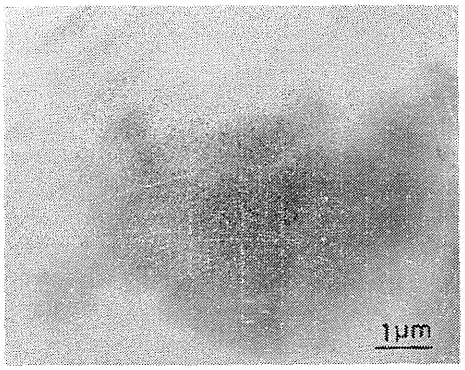

Fig. 47. Microstructure of electron-irradiated Ni.

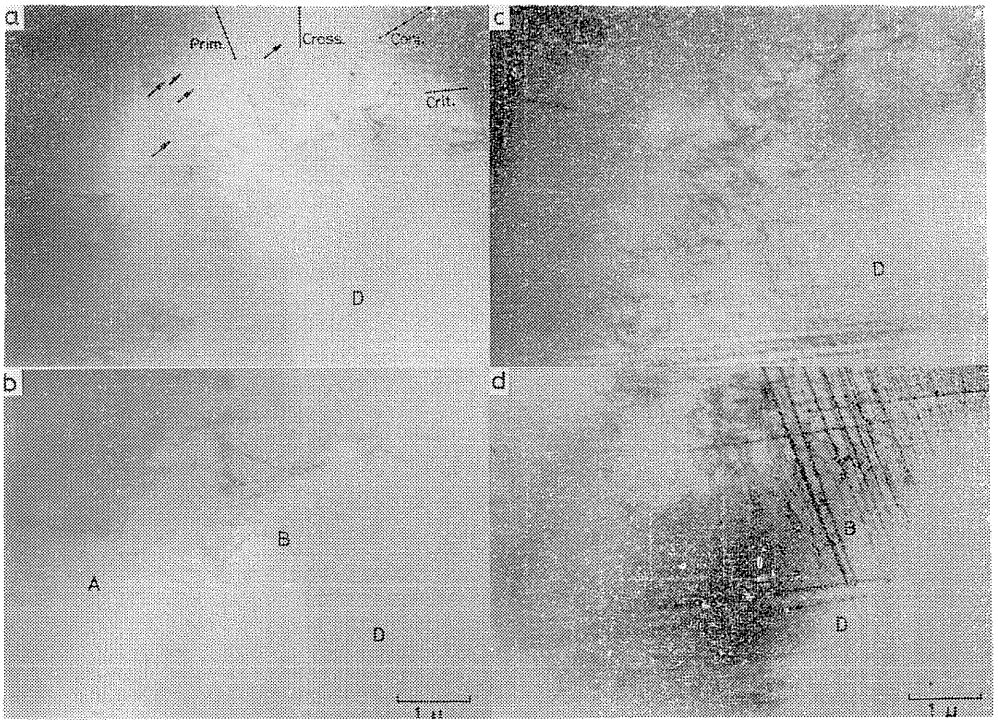

Fig. 48. Example of sequence of deformation in the damaged and in the undamaged regions of Ni.

vealed that the features of deformation of the damaged Ni were substantially different from those of the undamaged Ni.

Slips initiated in the undamaged region. Those dislocations which moved in the undamaged region were stopped near the boundary of the damaged region and could not penetrate into the damaged region at an early stage of deformation. This substantiates that stress necessary to move dislocations in the damaged region is larger than that in the undamaged region; this is a phenomenon known as radiation-hardening of metals. On further stressing, those dislocations which had been trapped at the boundary of the damaged region penetrated into the damaged region. The crystal inside the slip bands in the damaged region, *e. g.*, A and B appears white as compared with the matrix outside the slip bands, indicating that the radiation-produced defect clusters inside the bands have heen eliminated by the dislocations which moved in the slip bands. That is, the so-called dislocation channels are formed in the crystal where slip bands have passed. This dislocation channeling is more clearly shown in Fig. 49, where the radiation-produced defect clusters have been completely eliminated within the channels.

In the undamaged region slip systems having very low Schmid factor were observed to operate at an early stage of deformation. In contrast, the dislocation channels in the damaged region were formed by the slip bands which had high Schmid factor. Four slip traces corresponding to the primary, conjugate, critical and cross-slip systems were observed in the undamaged region of Fig. 48 (a), while in the damaged region only the primary and critical slip systems, both having Schmid factor about 0.45 in this case, operated and formed the dislocation channels. The cross-slip system (Schmid factor 0.16 in this case) was frequently observed in the undamaged region but never in the damaged region. The dislocations of cross-slip system which moved in the undamaged region changed their slip plane from the cross-slip plane to the primary slip plane near the boundary of the damaged region as can be seen from the slip trails of individual dislocations (indicated by arrows in Fig. 48 (a)).

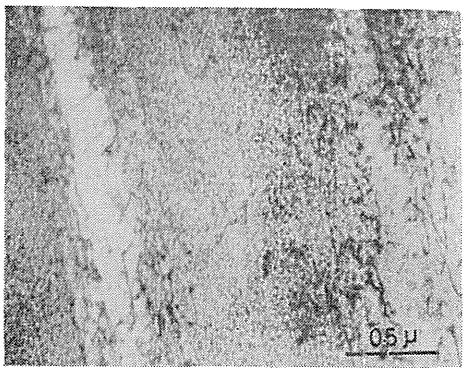

Fig. 49. Dislocation channels formed in electron-damaged Ni.

Furthermore, slip traces in the undamaged region were fine and homogeneous on electron microscopic scale, while in the damaged region coarse dislocation channels were formed heterogeneously. Many dislocation debris consisting of zigzagged dislocation lines and dislocation loops whose diameter was much larger than that of radiation-produced defect clusters were observed in the dislocation channels. To the contrary, only few smoothly curved dislocations remained in the deformed undamaged region. This feature of configuration of trapped dislocations is also true for moving dislocations in the damaged and in the undamaged regions. That is, in the damaged region the moving dislocations had the zigzagged shapes and they moved in a jerky manner, while in the undamaged region smoothly curved dislocations moved in a

smooth manner, as is shown in Fig. 50.[67] It is clear that dislocations experience a considerable resistance from the defect clusters.

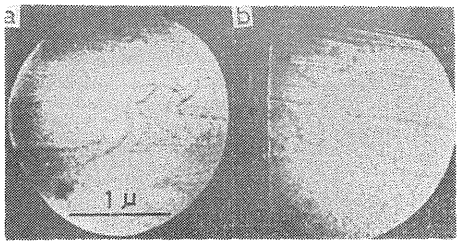

Fig. 50. (a) Motion of dislocations in an undamaged Ni.
(b) Motion of dislocations in an electron-damaged Ni.

6. 3. 2. Neutron-irradiated Ni

Fig. 51 is the micrograph showing the structure of an as-irradiated Ni (4.5×10^{18} n/cm^2). The defect clusters as small as tens Å to hundred Å in diameter are distributed uniformly in the matrix. The density was about 7×10^{15} /cm^3. Fig. 52 shows a sequence of the formation of slip bands in such a neutron-irradiated Ni

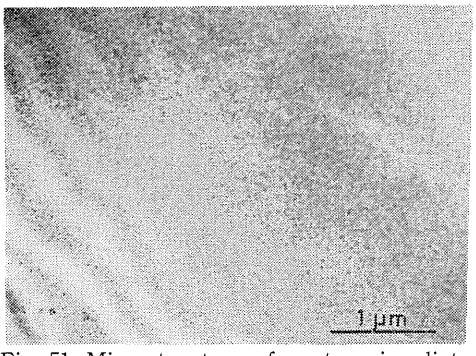

Fig. 51. Microstructure of neutron-irradiated Ni.

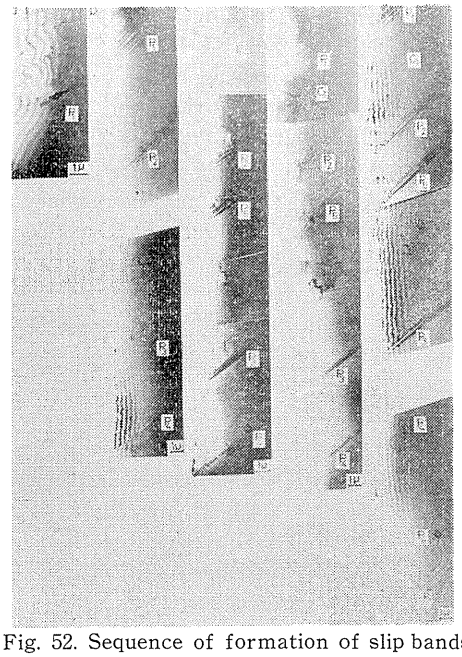

Fig. 52. Sequence of formation of slip bands in neutron-irradiated Ni.

which was stretched in HVEM. The slip bands about 0.2 μm in width were formed successively as the deformation proceeded. It is to be noted that a secondary slip was observed only at C' and that most of slip bands belonged to the primary slip system. It can be seen from Fig. 52 that the deformation is highly heterogeneous;

plastic strain is concentrated in the slip bands and the matrix between the slip bands remains undeformed.

Fig. 53 shows a process of the formation and hardening of a single dislocation channel at high magnification. The defect clusters in the channel were nearly completely eliminated even immediately after the channel was formed. At this stage the strain within the channel amounts to as large as 100%, as can be seen from the offset of equi-thickness fringes in Fig. 54. At a later stage of deformation, however, the dislocations moving in the channel were trapped by those defect clusters which survived near the periphery of the channel as is shown in Fig. 53 (b) and (c). Such trapped dislocations rendered strong barriers to the motion of the dislocations which followed in the channel. Thus, dislocations were accumulated progressively in the channel, resulting in hardening. At this stage strain in the channel got saturated and a fresh dislocation channel is formed at a distant place and strain is carried by the dislocations which move in the new channel. The same hardening process as described above is repeated for this channel

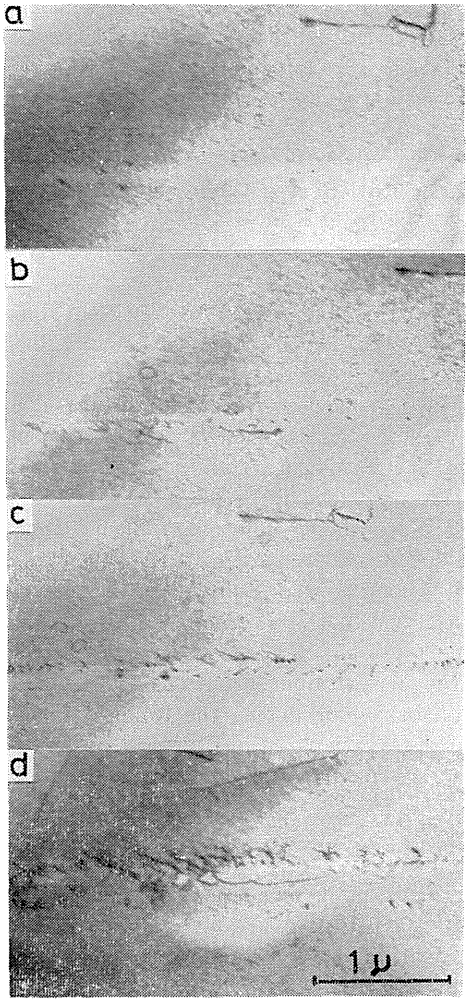

Fig. 53. Sequence of formation and hardening of a single dislocation channel in neutron-irradiated Ni.

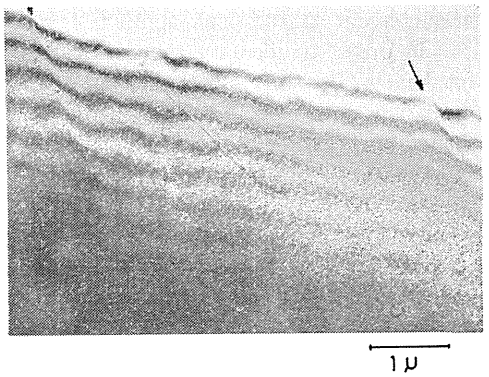

Fig. 54. Dislocation channels observed in neutron-irradiated Ni. Plastic strain is concentrated in the channels.

and thus, new channels are formed successively as deformation proceeds.

These observations suggest that the formation of dislocation channel is an exceedingly dynamic phenomenon and that many numbers of dislocations move cooperatively at the initial stage of deformation in dislocation channels. Most of strain is carried at this stage. At a later stage of dislocation channeling, only a small amount of strain is carried by the dislocations which move in the channel,

because the density of dislocations in the channel increases and the channel hardens.

Thus, a dislocation channel hardens spontaneously through the interaction of the dislocations of the primary slip plane alone with the defect clusters surviving in the channel. That is, the activity of dislocations moving on the slip planes other than the primary slip plane need not be invoked to explain the hardening of a dislocation channel.

The dynamic behaviour of dislocations in neutron-irradiated Ni was essentially similar to that of dislocations in electron-irradiated Ni.[68] Thus, it is expected that a combined *in-situ* experiment of irradiation and deformation in HVEM will render a powerful tool for the study of radiation hardening of metals and alloys.

7. Dislocation Behaviour during Push-Pull Stress Cycle in Ni

7. 1. Introduction

Fatigue-hardening of metals is somewhat more complex than the case of unidirectional work-hardening, mainly because of the added complications of load reversal and of load repetition.[69] TEM has been extensively used to observe the change in microstructure of metals during fatigue-hardening for the purpose of identifying the reversible process and the irreversible one involved in fatigue process. In these investigations, however, bulk crystals are fatigued, from which foil specimens for TEM are sliced. As has been already described in detail in Chapter 5, a substantial rearrangement of dislocations takes place during unloading. Such a rearrangement also takes place during thinning of specimen. As a result, the dislocation structures observed so far by conventional TEM method represent only the dislocation arrangement in the stress-removed state and not represent the dislocation arrangement at the peak applied stresses.

In order to identify the reversible and the irreversible processes of fatigue-hardening, dynamic observations of dislocation behaviour during the full range of a push-pull stress cycle will be required. Some observations of dislocation behaviour during a stress cycle have been carried out by an *in-situ* deformation experiment in HVEM.

7. 2. Experimental

Materials used in this study are single crystals grown from high-purity Ni (99.99%, Johnson Matthey and Co. Ltd.). Foil specimens were glued onto a substrate plate prior to the *in-situ* deformation experiment in HVEM. The substrate plate was in turn cycled in reverse bending and the specimen glued on it was strained in push-pull about the mean strain of zero.[70] These fatigued foil specimens were then detached from the substrate by dissolving the adhesive and slightly repolished to remove the surface steps associated with slip bands. Then, one additional push-pull stress cycle was applied to the specimen while under observation in HVEM with the aid of the alternate-straining device described in Sec. 2. 2. 5. (Fig. 55).

7. 3. Results

Fig. 56 shows a typical microstructure of a Ni foil specimen which was fatigue-strained through a reverse bending of a substrate plate on which the specimen was glued ($\varepsilon = \pm 0.002$, $N = 1000$). Well developed cell structure is observed and in

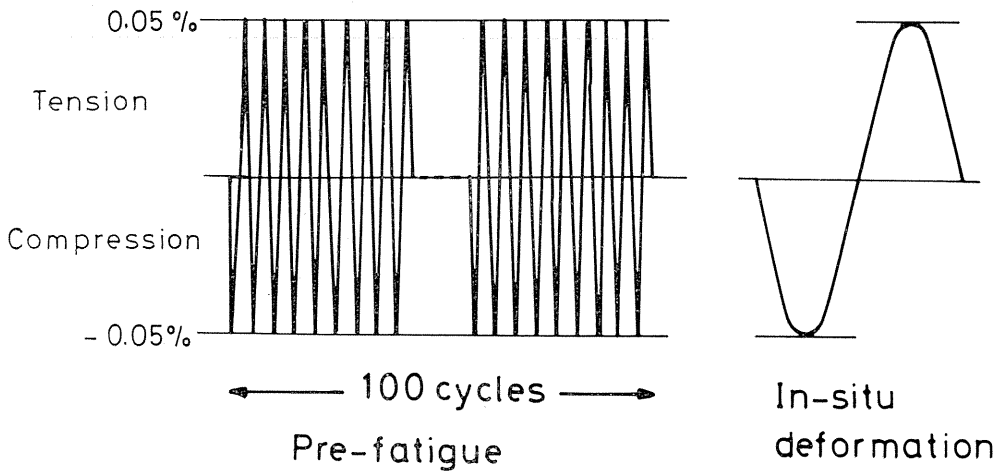

Fig. 55. Schematic illustration of the procedures of *in-situ* fatigue experiement in HVEM.

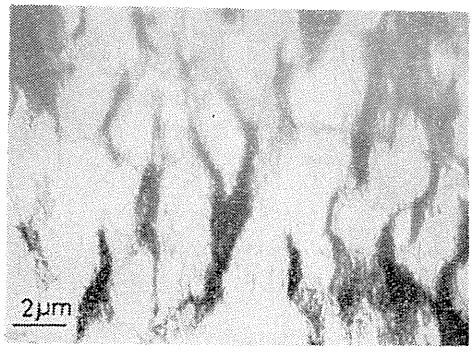

Fig. 56. A typical microstructure of a Ni specimen fatigue-hardened in foil state.

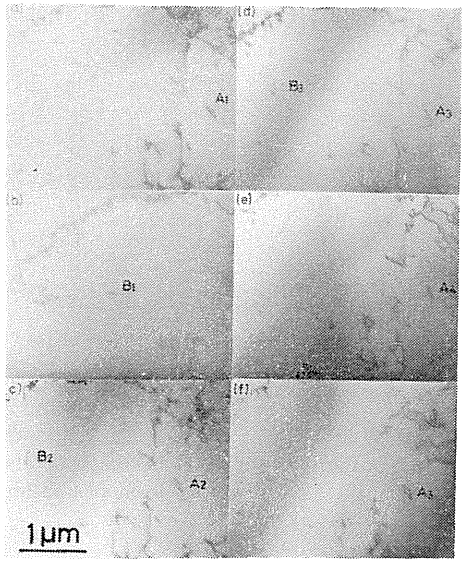

Fig 57. Variation in dislocation structure during compression-tension stress cycle in pre-fatigued Ni foil.

addition, a number of dipole patches, dislocation loops and long isolated dislocations connecting the cell walls are observed. These features of microstructures of a fatigued foil specimen have a strong resemblance to the features characteristic of the structure of fatigue-hardened metals in bulk state. This suggests that similar mechanisms operate both in foil crystal and in bulk crystal during fatigue-hardening. Thus, the validity of the present *in-situ* experiment using foil speimens is supported.

Fig. 57 shows a sequence of the dislocation arrangement at the same area of a

pre-fatigued Ni foil specimen ($\varepsilon = \pm 0.0005$, N=100) during a subsequent compression-tension stress cycle in HVEM. Cell structure developed during pre-fatigue was so stable that the change of their configurations during the subsequent stress cycle was negligibly small. Dislocations which happened to escape from the cell walls repeated reversible motion (shuttling motion). For example, dislocation B escaped from the cell wall and advanced into the interior of the cell as the compressional stress* was applied to the specimen (b). As the applied stress was changed from compression to tension, B became straight and finally moved backwards to the original place (d). Such a long-range reversible motion of a dislocation indicates that the stress acting on the dislocation was reversed over a wide range of crystal and that the foil specimen was actually subjected to a compression-tension stress cycle.

The behaviour of a dislocation loop A in Fig. 57 is shown at high magnification in Fig. 58 to show more clearly its change in configuration during the stress cycle.

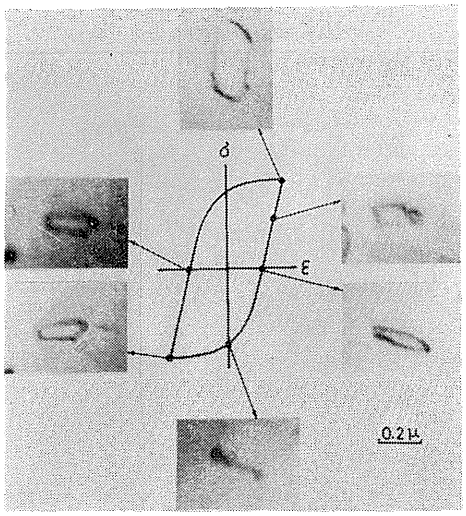

Fig. 58. Variation in shape of dislocation loop during compression-tension stress cycle in pre-fatigued Ni.

The separation between the two parallel long dislocation segments composing the loop oscillated as the stress was converted from compression to tension. This behaviour of a dislocation loop can be rationalized by considering the loop as a prismatic loop and also the edge components as repeating the so-called "flip-flop" motion proposed by Feltner.[71]

Although a detailed quantitative analysis cannot be made in this preliminary study, it is clear that a comprehensive *in-situ* fatigue experiment in HVEM will throw light on the elementary process of fatigue-hardening of metals.

---

* The pre-fatigue applied to this specimen was terminated by applying one half-stress cycle in tension side. As a result, applying a compressional stress in HVEM means that the specimen is strained in the reverse direction (cf. Fig. 55).

8. Conclusion and Remarks on Extending Works

Based on *in-situ* deformation experiments in a HVEM, a new direct method is developed and is used to investigate the dynamic properties of dislocations in various types of metal (bcc...Fe, Fe-3%Si, Mo, fcc...Ni) under various experimental conditions (stretched or compressed, low or high temperatures, electron- or neutron-irradiated or unirradiated). The important results obtained are as follows:

(1) By using the new method, a direct correlation between the dynamical behaviour of dislocations and the stress-strain behaviour of a crystal has been established for the first time.

(2) The mobilities of edge and screw dislocations in Fe, Fe-3%Si and Mo have been measured directly and it is found that the motion of screw dislocations in these bcc metals has a large temperature dependence and that the low mobility of screw dislocations actually controls the plasticity of these metals at low temperatures.

(3) Various kinds of dislocation source are observed. The mechanism and rate of multiplication of dislocations are analyzed.

(4) In zone-refined Mo, two types of anomalous slip, namely, one due to surface-effect mechanism and the other due to co-planar double slip mechanism operate actually.

(5) Estimation of local internal stress and frictional stress acting on each particular dislocations is successfully made by unloading-reloading stress cycle experiments.

(6) For the first time, shuttling motion and flip-flop motion of dislocations are observed by *in-situ* fatigue test in a HVEM successfully.

(7) Formation of dislocation channels is observed directly by the *in-situ* deformation experiment on electron- or neutron-irradiated Ni in HVEM.

Remarks on Extending Works

To carry out the *in-situ* experiments in a controlled atmosphere, a new type of an environmental cell for use with a HVEM has been constructed. This cell can be used as a window type of cell and also can be used, if necessary, as a differential pumping type of cell. By using this cell, preliminary experiments on the structure change of amorphous selenium during heating (amorphous state $\rightarrow$ crystalline state $\rightleftarrows$ liquid state) have been carried out successfully. The application of this cell to the *in-situ* studies on deformation, stress corrosion and hydrogen embrittlement is now being planned.

As regards the microscopic mechanisms of yielding[74], the dynamical formation and fragmentation of cell structure[75] (a type of dislocation structure in work-hardened crystals) and the dynamic formation and propagation of cracks in foil specimens[76], some of the results have been already reported. However, since it is thought that a comprehensive report on these subjects should be made after the systematic studies have been completed on a variety of metals under various experimental conditions, these subjects are excluded in this text.

Improvement of the resolution and of the recording speed of the EM images of moving dislocations with the aid of modern imaging as well as image-processing techniques is now in progress.

Acknowledgements

The present authors would like to express their hearty thanks to Messrs K. Noda, K. Matsumoto and A. Yamamoto for their co-operation in carrying out the experiments. Thanks are also due to Dr. N. Yukawa, Messrs. A. Nohara, N. Okamoto and T. Tono for the stimulating discussions and the contributions in constructing some of the attachments. The works on high-purity Mo were performed in co-operation with Dr. H. Matsui and Prof. H. Kimura of Tohoku University. The authors are also indebted to Messrs. I. Ishikawa, S. Kashikura, K. Miyauchi and S. Katagiri of Hitachi Ltd. in constructing some of the devices. Dr. T. Takeuchi of National Research Institute for Metals kindly supplied iron single crystals. Dr. I. Igarashi of Toyota Research and Development Laboratories Inc. supplied the semiconductor strain gauges TENPAC. The authors wish to express their hearty thanks to Dr. K. Shiraishi of JAERI for his kind helps in performing the *in-situ* experiment on neutron-irradiated Ni at JAERI. They are also indebted to Dr. H. Yoshida of Kyoto University for making neutron-irradiation possible. Thanks are also due to Dr. M. Iseki for helpful advices in treating irradiated Ni. Finally the authors acknowledge the members of HVEM group of Nagoya University, Messrs. M. Nonoyama, C. Morita, S. Arai and T. Goto for their assistances in operating the high voltage electron microscopes (HU-500 and HU-1000D).

References

1) Johnston, W. G. and J. J. Gilman : J. appl. Phys. **30** (1959) 129.
2) Stein, D. F. and J. R. Low, Jr. : J. appl. Phys. **31** (1960) 362.
3) Suzuki, T. and H. Kojima : Acta Met. **14** (1966) 913.
4) Saka, H. and T. Imura : J. Phys. Soc. Japan **32** (1972) 702.
5) Uyeda, R. and M. Nonoyama : Japan. J. appl. Phys. **6** (1967) 557; *Ibid.*, **7** (1968) 200.
6) for example, T. Imura,: in "*High Voltage Electron Microscopy*" edited by P. R. Swann *et al.*, p. 179. Academic Press, London (1974).
7) Saka, H., T. Imura and N. Yukawa : Japan. J. appl. Phys. **10** (1971) 1.
8) Takahashi, N., K. Ashinuma, M. Watanabe, I. Okazaki, and Y. Nagahama : J. Electron Microscopy **9** (1960) 104.
9) Saka, H., K. Noda and T. Imura: Japan. J. appl. Phys. **11** (1972) 1039; J. Phys. Soc. Japan **32** (1972) 289.
10) Nohara, A., N. Yukawa, M. Yokoi, I. Ishikawa, and T. Imura : Japan. J. appl. Phys. **14** (1975) 1829.
11) Nohara, A. and T. Imura : Japan. J. appl. Phys. **11** (1972) 1039.
12) Nohara, A., N. Yonezawa, T. Chikada, N. Yukawa and T. Imura : Proc. 8th Int. Cong. on EM, Canberra, 1974 "*Electron Microscopy*" **1** (1974) 570.
13) Saka, H., A. Yamamoto, K. Noda and T. Imura : Japan. J. appl. Phys. **15** (1976) 1977.
14) Imura, T. *et al.* : Proc. 8th Int. Cong. on EM, Canberra, 1974 "*Electron Microscopy*", **1** (1974) 570.
15) Price, P. B. : Phil. Mag. **5** (1960) 417; Proc. Roy. Soc. **A 260** (1961) 251; Phil. Mag. **5** (1960) 873; *Ibid.* **6** (1961) 243.
16) Price, P. B. : J. appl. Phys. **32** (1961) 1746, 1750.
17) Crump III, J. C. and J. W. Mitchell : J. appl. Phys. **41** (1970) 717.
18) Imura, T. : in "*Electron Microscopy and Structure of Materials*" edited by G. Thomas *et al.*, p. 104, Univ. California Press, 1972.
19) Wilsdorf, H. G. F. : in "*Structure and Properties of Thin Film*" edited by C. A. Neugebauer *et al.*, p. 151, John Wiley & Sons, New York, 1960.

20) Fujita, H. and H. Yamada : Trans. Japan Inst. Metals **9** (1968), Suppl. p. 943.
21) Furubayashi, E. : Trans. Japan Inst. Metals **9** (1968), Suppl. p. 939 ; J. Phys. Soc. Japan **27** (1969) 130.
22) Ikeda, S. : Japan. J. appl. Phys. **9** (1972) 1273 ; *Ibid.* **13** (1974) 779.
23) Ikeno, S. and E. Furubayashi : Phys. stat. solidi (a) **12** (1972) 611 ; *Ibid.* **27** (1975) 581.
24) Saka, H. and T. Imura : Japan. J. appl. Phys. **8** (1969) 406.
25) Saka, H. : in "*Jikken Butsurigaku Koza, Vol. 11, Koshi-Kekkan* (Lattice Defects)" edited by H. Suzuki, Kyoritsu-Shuppan, Tokyo, to be published (in Japanese).
26) Nohara, A., N. Yukawa, M. Yokoi and T. Imura : Japan. J. appl. Phys. **12** (1973) 157.
27) Hirsch, P. B., A. Howie, R. B. Nicholson, D. W. Pashley and M. J. Whelan : "*Electron Microscopy of Thin Crystals*" p. 81, Butterworths, London, 1965.
28) Imura, T., H. Saka, H. Todokoro, and M. Ashikawa : J. Phys. Soc. Japan **31** (1971) 1849.
29) Ashikawa, M., H. Todokoro, H. Takemoto and H. Saka : Television **25** (1971) 948 (in Japanese).
30) Imura, T., H. Saka, M. Doi and N. Okamoto : Japan. J. appl. Phys. **10** (1971) 654.
31) Hirsch, P. B. : Trans. Japan Inst. Metals **9** (1968), Suppl. p. XXX.
32) Christian, J. W. : Proc. 2 nd Int. Conf. on the Strength of Metal and Alloys, Asilomar, Vol. 1. p. 31.
33) Imura, T. : Proc. 4 th Int. Conf. on HVEM, 1975, Toulouse, "*Microscopie Electronique a Haute Tension*" edited by B. Jouffrey and P. Favard, p. 293, Societe Francaise de Microscopie Electronique, Paris, 1976.
34) Saka, H., K. Noda and T. Imura : Crystal Lattice Defects **4** (1973) 45.
35) Noda, K., H. Matsui, H. Saka, H. Kimura and T. Imura : to be published.
36) Marukawa, K. : J. Phys. Soc. Japan **22** (1967) 499.
37) Vreeland, T. : in "*Direct Observation of Structure and Imperfections*" edited by R. E. Bunshan, p. 341, Interscience, New York (1968).
38) Saka, H. and T. Imura : Phys. stat. solidi (a) **19** (1973) 653.
39) Imura, T. and S. Takeda : J. Phys. Soc. Japan **26** (1969) 1326.
40) Saka, H., K. Noda and T. Imura : Trans. Iron and Steel Inst. Japan **13** (1973) 319.
41) Takeuchi, T. : J. Phys. Soc. Japan **26** (1969) 354.
42) Taylor, G., R. Bajaj and O. N. Carlson : Phil. Mag. **28** (1973) 1035.
43) Duesberry, M. S. and R. A. Foxall : Phil. Mag. **20** (1969) 719.
44) Bolton, D. K. and G. Taylor : Phil. Mag. **26** (1972) 1357.
45) Louchet, F. and L. P. Kubin : Acta Met. **23** (1975) 17.
46) Takeuchi, S., E. Kuramoto and T. Suzuki : Acta Met. **20** (1972) 909.
47) Vesely, D. : Phys. stat. solidi **29** (1968), 675, 685.
48) Matsui, H. and H. Kimura : to be published in Mat. Sci. Eng.
49) Kaun, L., A. Luft, J. Richer and D. Schulze : Phys. stat. solidi **26** (1968) 485.
50) Takeuchi, S. and E. Kuramoto : Scripta Met. **8** (1974) 785.
51) Matsui, H. and H. Kimura : Scripta Met. **7** (1973) 905.
52) Matsui, H., H. Saka, K. Noda, H. Kimura and T. Imura : Scripta Met. **8** (1974) 1205.
53) Matsui, H. and H. Kimura : Scripta Met. **9** (1975) 971.
54) Louchet, F. and L. P. Kubin : Scripta Met. **9** (1975) 911.
55) Crump III, J. C. and F. W. Young, Jr. : Phil. Mag. **17** (1967) 381.
56) Mughrabi, H. : Phil. Mag. **18** (1968) 1211 ; *Ibid.*, **23** (1971) 869, 895, 931.
57) Saka, H., K. Noda, K. Matsumoto and T. Imura : Scripta Met. **10** (1976) 29.
58) Noda, K., H. Saka, H. Matsui, H. Kimura and T. Imura : Proc. 4 th Int. Conf. on HVEM, 1975, Toulouse, "*Microscopie Electronique a Haute Tension*" edited by B. Jouffrey and P. Farvard, p. 321, 1976.
59) Wechsler, M. S. : in "*The Inhomogeneity of Plastic Deformation*" edited by R. E. Reed-Hill, ASM, Ohio, p. 19, 1972.
60) Makin, M. J. : Phil. Mag. **18** (1968) 637.
61) Wilkens, M. and K. Urban : in "*High Voltage Electron Microscopy*" edited by P. R. Swann, p. 332, Academic Press, London, 1974.

62) Kiritani, M. and N. Yoshida : Crystal Lattice Defects, **4** (1973) 83.
63) Saka, H., K. Noda, K. Matsumoto and T. Imura : Japan. J. appl. Phys. **12** (1973) 1643.
64) Saka, H., K. Noda, K. Matsumoto and T. Imura : Phys. stat. solidi (a) **31** (1975) 139.
65) Saka, H., K. Noda, K. Shiraishi, H. Yoshida and T. Imura : unpublished work.
66) Urban, K. : Phys. stat. solidi (a) **4** (1971) 761.
67) Saka, H., K. Noda, K. Matsumoto and T. Imura : Scripta Met. **9** (1975) 499.
68) Saka, H., K. Noda, K. Matsumoto and T. Imura : Proc. 4 th Int. Conf. on HVEM, *"Electronique Microscopie a Haute Tension"* edited by B. Jouffrey and P. Favard, p. 325, 1976.
69) Grosskreutz, J. C. : Phys. stat. solidi (b) **47** (1971) 11.
70) Grosskreutz, J. C. and P. Waldow : Acta Met. **11** (1963) 717.
71) Feltner, C. E.: Phil. Mag. **12** (1965) 1225.
72) Saka, H., H. Matsui, K. Noda, H. Kimura and T. Imura : Scripta Met. **10** (1976) 59.
73) Saka, H., K. Noda, T. Imura, H. Matsui and H. Kimura : Phil. Mag. **34** (1976), 33.
74) Saka, H., M. Doi and T. Imura : J. Phys. Soc. Japan **30** (1971) 1503.
75) Imura, T., H. Saka and N. Yukawa : Japan. J. appl. Phys. **8** (1969) 405.
76) Saka, H. and T. Imura : Japan. J. appl. Phys. **9** (1970) 1185.
77) Nohara, A., K. Muramoto, N. Yukawa and T. Imura : unpublished work.